53. Wang, J.; Lu, J.; Olsen, K., *Analyst* **117**, 1913 (1992).
54. Hutton, E.; van Elteren, J.; Ogorevc, B.; Smyth, M., *Talanta* **63**, 849 (2004).
55. Gottesfeld, S.; Ariel, M., *J. Electroanal. Chem.* **9**, 112 (1965).
56. Wang, J.; Mannino, S., *Analyst* **114**, 643 (1989).
57. Obata, H.; van den Berg C. M. C., *Anal. Chem.* **73**, 2522 (2001).
58. Ostapczuk, P., *Clin. Chem.* **38**, 1995 (1992).
59. Lai, P.; Fung, K., *Analyst* **103**, 1244 (1978).
60. Golimowski, J.; Gustavsson, I., *Fres. Z. Anal. Chem.* **317**, 484 (1984).
61. Adeloju, S. B.; Bond, A. M.; Briggs, M. H., *Anal. Chim. Acta* **164**, 181 (1984).
62. Hoppstock, K.; Michulitz, M., *Anal. Chim. Acta* **350**, 135 (1997).
63. Porbes, S.; Bound, G.; West, T., *Talanta* **26**, 473 (1979).
64. Levit, D. I., *Anal. Chem.* **45**, 1291 (1973).
65. Wang, J.; Setiadji, R.; Chen, L.; Lu, J.; Morton, S., *Electroanalysis* **4**, 161 (1992).
66. Williams, T.; Foy, O.; Benson, C., *Anal. Chim. Acta* **75**, 250 (1975).
67. Cavicchioli, A.; La-Scalea, M. A.; Gutz, I. G., *Electroanalysis* **16**, 697 (2004).
68. Florence, T. M., *Analyst* **111**, 489 (1986).
69. Wang, J., *Analyst* **119**, 763 (1994).
70. Tercier, M. L.; Buffle, J.; Graziottin, F., *Electroanalysis* **10**, 355 (1998).
71. Wang, J., *Anal. Chim. Acta* **500**, 247 (2003).
72. Moane, S.; Park, S.; Lunte, C. E.; Smyth, M. R., *Analyst* **123**, 1931 (1998).
73. Ewing, A. G.; Mesaros, J. M.; Gavin, P. F., *Anal. Chem.* **66**, 527A (1994).
74. Curry, P.; Engstrom, C.; Ewing, A., *Electroanalysis*, **3**, 587 (1991).
75. Holland, L. A.; Lunte, S. M., *Anal. Commun.* **35**, 1H (1998).
76. Sloss, S.; Ewing, A. G., *Anal. Chem.* **63**, 577 (1993).
77. Woolley, A.; Lao, K.; Glazer, A.; Mathies, R., *Anal. Chem.* **70**, 684 (1998).
78. Wang, J., *Electroanalysis* **17**, 1133 (2005).
79. Lacher, N. A.; Garrison, K. E.; Martin, R. S.; Lunte, S. M., *Electrophoresis* **22**, 2526 (2001).
80. Woolley, T.; Lao, K.; Glazer, A. N.; Mathies, R. A., *Anal. Chem.* **70**, 684 (1998).
81. Wang, J.; Tian, B.; Sahlin, E., *Anal. Chem.* **71**, 5436 (1999).
82. Hilmi, A.; Luong, J. H., *Anal. Chem.* **72**, 4677 (2000).
83. Chen, D.; Hsu, F.; Zhan, D.; Chen, C., *Anal. Chem.* **73**, 758 (2001).
84. Hanekamp, H. B.; Box, P.; Frei, R. W., *Trends Anal. Chem.* **1**, 135 (1982).
85. Trojanek, A.; De Jong, H. G., *Anal. Chim. Acta* **141**, 115 (1982).
86. Johnson, D. C.; LaCourse, W. R., *Anal. Chem.* **62**, 589A (1990).
87. Johnson, D.C.; LaCourse, W. R., *Electroanalysis* **4**, 367 (1992).
88. LaCourse, W. R., *Pulsed Electrochemical Detection in HPLC*, Wiley, New York, 1997.
89. Roston, D. A.; Shoup, R. E.; Kissinger, P. T., *Anal. Chem.* **54**, 1417A (1982).
90. Hoogvliet, J.; Reijn, J.; van Bennekom, W., *Anal. Chem.* **63**, 2418 (1991).
91. Stulik, K.; Pacáková, V., *Electroanalytical Measurements in Flowing Liquids*, Ellis Horwood, Chichester, UK, 1987.
92. Warner, M., *Anal. Chem.* **66**, 601A (1994).

4

PRACTICAL CONSIDERATIONS

The basic instrumentation required for controlled-potential experiments is relatively inexpensive and readily available commercially. The basic necessities include a cell (with a three-electrode system), a voltammetric analyzer (consisting of a potentiostatic circuitry and a voltage ramp generator), and a plotter. Modern voltammetric analyzers are versatile enough to perform many modes of operation. Depending on the specific experiment, other components may be required. For example, a faradaic cage is desired for work with ultramicroelectrodes. The system should be located in a room free from major electrical interferences, vibrations, and drastic fluctuations in temperature.

4.1 ELECTROCHEMICAL CELLS

Three-electrode cells (e.g., see Fig. 4.1) are commonly used in controlled-potential experiments. The cell is usually a covered beaker of 5–50 mL volume, and contains the three electrodes (working, reference, and auxiliary), which are immersed in the sample solution. While the working electrode is the electrode at which the reaction of interest occurs, the reference electrode provides a stable and reproducible potential (independent of the sample composition), against which the potential of the working electrode is compared. Such "buffering" against potential changes is achieved by a constant composition of both forms of its redox couple, such as Ag/AgCl or Hg/Hg_2Cl_2, as common

Analytical Electrochemistry, Third Edition, by Joseph Wang

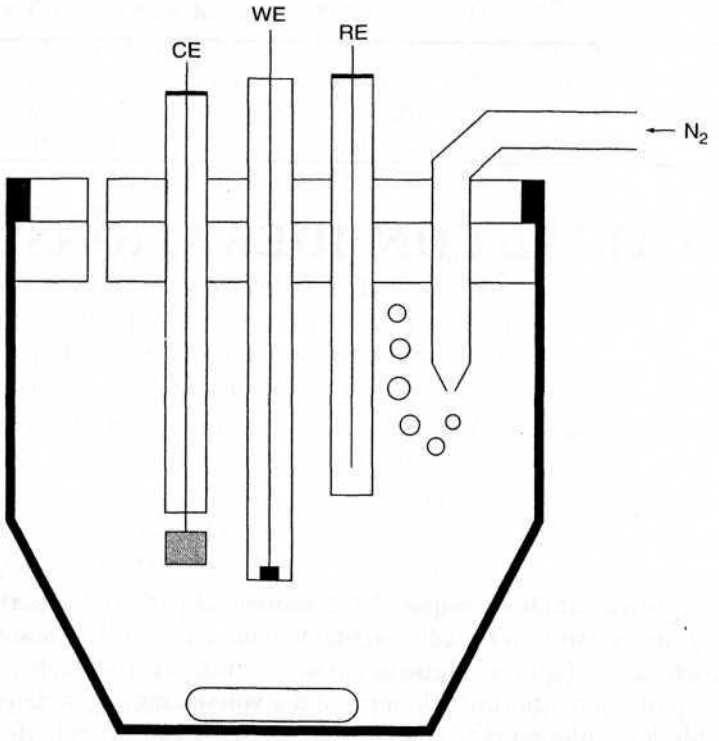

Figure 4.1 Schematic diagram of a cell for voltammetric measurements: WE—working electrodes; RE—reference electrode; CE—counter electrode. The electrodes are inserted through holes in the cell cover.

with the silver–silver chloride and the saturated calomel reference electrodes, respectively. To minimize contamination of the sample solution, the reference electrode may be insulated from the sample through an intermediate bridge. An inert conducting material, such as platinum wire or graphite rod, is usually used as the current-carrying auxiliary electrode. The relative position of these electrodes and their proper connection to the electrochemical analyzer should be noted (see Section 4.4). The three electrodes, as well as the tube used for bubbling the deoxygenating gas (see Section 4.3), are supported in five holes in the cell cover. Complete systems, integrating the three-electrode cell, built-in gas control, and magnetic stirrer, along with proper cover, are available commercially (e.g., see Fig. 4.2).

The exact cell design and the material used for its construction are selected according to the experiment at hand and the nature of the sample. The various designs differ with respect to size, temperature control capability, stirring requirement, shape, or number of cell compartments. Various microcells with 20–500 μL volumes can be used when the sample volume is limited. Particularly attractive are thin-layer cells in which the entire sample is confined within

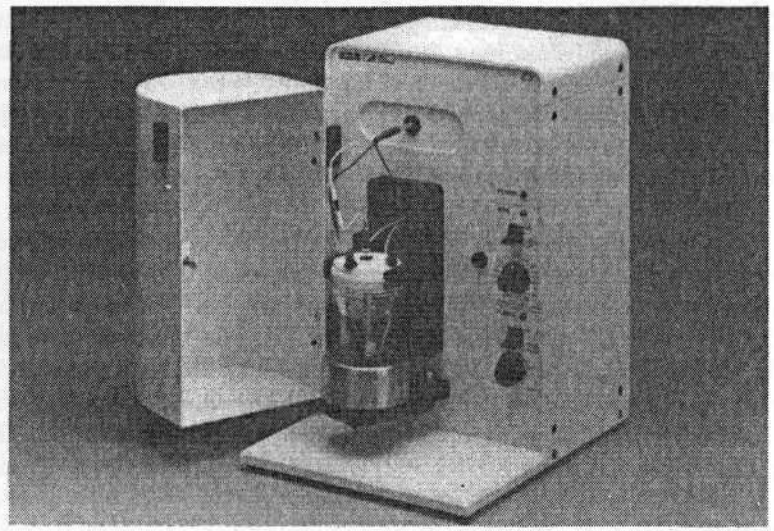

Figure 4.2 A complete cell stand. (Courtesy of BAS Inc.)

a thin layer (of less than 10 μm thickness) at the electrode surface (1). Smaller sample volumes can be accommodated in connection with ultramicroelectrodes (discussed in Section 4.4) and advanced microfabrication processes (discussed in Section 6.3). In particular, lithographically fabricated picoliter microvials (2) hold great promise for assays of ultrasmall environments (e.g., single-cell systems). Specially designed flow cells (discussed in Section 3.6) are used for on-line applications. Glass is commonly used as the cell material, due to its low cost, transparency, chemical inertness, and impermeability. Teflon and quartz represent other possible cell materials. The cell cover can be constructed of any suitable material that is inert to the sample. An accurate temperature control is readily achieved by immersing or jacketing the cell in a constant-temperature bath.

4.2 SOLVENTS AND SUPPORTING ELECTROLYTES

Electrochemical measurements are commonly carried out in a medium that consists of solvent containing a supporting electrolyte. The choice of solvent is dictated primarily by the solubility of the analyte and its redox activity, and by solvent properties, such as the electrical conductivity, electrochemical activity, and chemical reactivity. The solvent should not react with the analyte (or products) and should not undergo electrochemical reactions over a wide potential range.

While water has been used as a solvent more than any other medium, nonaqueous solvents [e.g., acetonitrile, propylene carbonate, dimethylformamide

(DMF), dimethylsulfoxide (DMSO), or methanol] have also frequently been used. Mixed solvents may also be considered for certain applications. Double-distilled water is adequate for most work in aqueous media. Triple-distilled water is often required when trace (stripping) analysis is concerned. Organic solvents often require a drying or purification procedure. These and other solvent-related considerations have been reviewed by Mann (3).

Supporting electrolytes are required in controlled-potential experiments to decrease the resistance of the solution, eliminate electromigration effects, and maintain a constant ionic strength (i.e., "swamping out" the effect of variable amounts of naturally occurring electrolyte) (4). The inert supporting electrolyte may be an inorganic salt, a mineral acid, or a buffer. While potassium chloride or nitrate, ammonium chloride, sodium hydroxide, or hydrochloric acid are widely used when water is employed as a solvent, tetraalkylammonium salts are often employed in organic media. Buffer systems (such as acetate, phosphate, or citrate) are used when a pH control is essential. The composition of the electrolyte may affect the selectivity of voltammetric measurements. For example, the tendency of most electrolytes to complex metal ions can benefit the analysis of mixtures of metals. In addition, masking agents [such as ethylenediaminetetraacetic acid (EDTA)] may be added to "remove" undesired interferences. The supporting electrolyte should be prepared from highly purified reagents, and should not be easily oxidized or reduced (hence minimizing potential contamination or background contributions, respectively). The usual electrolyte concentration range is 0.1–1.0 M, i.e., in large excess of the concentration of all electroactive species. Significantly lower levels can be employed in connection with ultramicroscale working electrodes (see Section 4.5.4).

4.3 OXYGEN REMOVAL

The electrochemical reduction of oxygen usually proceeds via two well-separated two-electron steps. The first step corresponds to the formation of hydrogen peroxide

$$O_2 + 2H^+ + 2e^- \rightarrow H_2O_2 \qquad (4.1)$$

and the second step corresponds to the reduction of the peroxide:

$$H_2O_2 + 2H^+ + 2e^- \rightarrow 2H_2O \qquad (4.2)$$

The half-wave potentials of these steps are approximately –0.1 and –0.9 V (vs. the saturated calomel electrode). The exact stoichiometry of these steps is dependent on the medium. The large background current accrued from this stepwise oxygen reduction interferes with the measurement of many reducible

analytes. In addition, the products of the oxygen reduction may affect the electrochemical process under investigation.

A variety of methods have thus been used for the removal of dissolved oxygen (5). The most common method has been purging with an inert gas (usually purified nitrogen) for 4–8 min prior to recording of the voltammogram. Longer purge times may be required for large sample volumes or for trace measurements. To prevent oxygen from reentering, the cell should be blanketed with the gas while the voltammogram is being recorded. Passage of the gas through a water-containing presaturator is desired to avoid evaporation. The deaeration step, although time-consuming, is quite effective and suitable for batch analysis. (The only exception is work with microsamples, where deoxygenation may lead to errors caused by the evaporation of solvent or loss of volatile compounds.)

Other methods have been developed for the removal of oxygen (particularly from flowing streams). These include the use of electrochemical or chemical (zinc) scrubbers, nitrogen-activated nebulizers, and chemical reduction (by addition of sodium sulfite or ascorbic acid). Alternately, it may be useful to employ voltammetric methods that are less prone to oxygen interference. The background-correction capability of modern (computerized) instruments is also effective for work in the presence of dissolved oxygen.

4.4 INSTRUMENTATION

Rapid advances in microelectronics, and in particular the introduction of operational amplifiers, have led to major changes in electroanalytical instrumentation. Tiny and inexpensive integrated circuits can now perform many functions that previously required very large instruments. Such trends have been reviewed (6). Various voltammetric analyzers are now available commercially from different sources (Table 4.1) at relatively modest prices [ranging from $5000 to $25,000 (in 2005)]. Such instruments consist of two circuits: a polarizing circuit that applies the potential to the cell, and a measuring circuit that monitors the cell current. The characteristic of modern voltammetric analyzers is the potentiostatic control of the working electrode, which minimizes errors due to cell resistance (i.e., poorly defined voltammograms with lower current response and shifted and broadened peaks). Equation 4.3 explains the cause for this ohmic distortion:

$$E_{app} = E_{WE} - E_{RE} - iR \qquad (4.3)$$

where iR is the ohmic potential drop.

The potentiostatic control, aimed at compensating a major fraction of the cell resistance, is accomplished with a three-electrode system and a combination of operational amplifiers and feedback loops (Fig. 4.3). Here, the reference electrode is placed as close as possible to the working electrode and

TABLE 4.1 Current Suppliers of Voltammetric Analyzers

Supplier	Address
Analytical Instrument Systems	PO Box 458 Flemington, NJ 08822 www.aishome.com
Bioanalytical Systems	2701 Kent Ave. W. Lafayette, IN 47906 www.bioanalytical.com
Cypress	PO Box 3931 Lawrence, KS 66044 www.cypresshome.com
CH Instruments	3700 Tennison Hill Dr. Austin, TX 78733 chinstr@worldnet.att.net
ECO Chemie	PO Box 85163 3508 AD Utrecht The Netherlands autolab@ecochemie.nl www.brinkmann.com
EG&G PAR	801 S. Illinois Ave. Oak Ridge, TN 37830 www.egg.inc.com/par
ESA	45 Wiggins Ave. Bedford, MA 01730
Metrohm	CH-9109 Herisau Switzerland www.brinkmann.com
Palm Instruments BV	Ruitercamp 119 3993 BZ Houten The Netherlands www.palmsens.com
Radiometer/Tacussel	27 rue d'Alscace F-69627 Villeurbanne France Analytical@clevelandOH.com
Solartron	964 Marcon Blvd. Allentown, PA 18103, USA www.solartron.com
TraceDetect	Seattle, WA, USA www.tracedetect.com

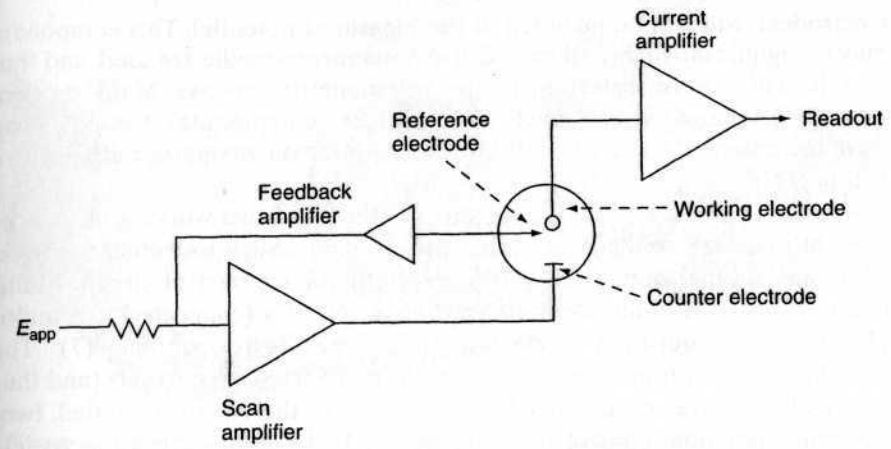

Figure 4.3 Schematic diagram of a three-electrode potentiostat.

connected to the instrument through a high-resistance circuit that draws no current from it. Because the flow cannot occur through the reference electrode, a current-carrying auxiliary electrode is placed in the solution to complete the current path. Hence, the current flows through the solution between the working and the auxiliary electrodes. Symmetry in the placement of these electrodes is important for the assumption that the current paths from all points on the working electrode are equivalent. Because no current passes through the reference electrode and because of its position close to the working electrode, the potential drop caused by the cell resistance (iR) is minimized. If the potential sensed by the reference electrode is less than the desired value, the operational amplifier control loop provides a corrective potential. By adding an operational amplifier current-to-voltage converter (called a "current follower") to the working electrode, it is possible to measure the current without disturbing the controlled parameters. The instrument also includes a ramp generator to produce various regularly changing potential waveforms.

As was pointed out earlier, an effective potential control requires a very close proximity between the working and reference electrodes. This can be accomplished by using a specially designed bridge of the reference electrode, known as a *Luggin probe*. The tip of this bridge should be placed as close as twice its diameter to the working electrode. A smaller distance will result in blockage (shielding) of the current path and hence a nonhomogeneous current density. The Luggin bridge should also not interfere to the convective transport toward the surface of the working electrode.

It should be pointed out that not all of the iR drop is removed by the potentiostatic control. Some fraction, denoted as iR_u (where R_u is the uncompensated solution resistance between the reference and working

electrodes), will still be included in the measured potential. This component may be significantly large when resistive nonaqueous media are used, and thus may lead to severe distortion of the voltammetric reponse. Many modern instruments, however, automatically subtract (compensate) the iR_u drop from the potential signal given to the potentiostat via an appropriate positive feedback.

Biopotentiostats, offering simultaneous control of two working electrodes (e.g., in ring–disk configuration) are also available. Such instruments consist of a conventional potentiostat with a second voltage-control circuit. Multipotentiostats, controlling multiple working electrodes (connected to a multiplexed data acquisition circuitry), have also been described (7). The development of ultramicroelectrodes, with their very small currents (and thus negligible iR losses even when R is large), allows the use of simplified, two-electrode, potential control (see Section 4.5.4). In contrast, ultramicroelectrode work requires an efficient current measurement circuitry to differentiate between the faradaic response and the extraneous electronic noise and for handling low currents down to the pA (picoampere) range. Other considerations for noise reduction involve the grounding and shielding of the instrument and cell.

The advent of inexpensive computing power has changed dramatically the way voltammetric measurements are controlled and data are acquired and manipulated. Computer-controlled instruments, available from most manufacturers (6), provide flexibility and sophistication in the execution of a great variety of modes. In principle, any potential waveform that can be defined mathematically can be applied with commands given through a keyboard. Such instruments offer various data processing options, including autoranging, blank subtraction, noise reduction, curve smoothing, differentiation, integration, and peak search. The entire voltammogram can be presented as a plot or printout (of the current–potential values). In addition, computer control has allowed automation of voltammetric experiments and hence has greatly improved the speed and precision of the measurement. Since the electrochemical cell is an analog element, and computers work only in the digital domain, analog-to-digital (A/D) and digital-to-analog (D/A) converters are used to interface between the two. Unattended operation has been accomplished through the coupling of autosamplers and microprocessor-controlled instruments (e.g., see Fig. 4.4). The autosampler can accommodate over 100 samples, as well as relevant standard solutions. Such coupling can also address the preliminary stages of sample preparation (as dictated by the nature of the sample). The role of computers in electroanalytical measurements and in the development of "smarter" analyzers has been reviewed by Bond (8) and He et al. (9).

The nature of electrochemical instruments makes them very attractive for decentralized testing. For example, compact, battery-operated voltammetric analyzers, developed for on-site measurements of metals (e.g., 10,11), readily address the growing needs for field-based environmental studies and security

Figure 4.4 Microprocessor-controlled voltammetric analyzer, in connection with an autosampler. (Courtesy of Metrohm Inc.)

surveillance applications. Similarly, portable (hand-held) instruments are being designed for decentralized clinical testing (12).

4.5 WORKING ELECTRODES

The performance of the voltammetric procedure is strongly influenced by the working-electrode material. The working electrode should provide high signal-to-noise characteristics, as well as a reproducible response. Thus, its selection depends primarily on two factors: the redox behavior of the target analyte and the background current over the potential region required for the measurement. Other considerations include the potential window, electrical conductivity, surface reproducibility, mechanical properties, cost, availability, and toxicity. A range of materials have found application as working electrodes for electroanalysis. The most popular are those involving mercury, carbon, or noble metals (particularly platinum and gold). Figure 4.5 displays the accessible potential window of these electrodes in various solutions. The geometry of these electrodes must also be considered.

4.5.1 Mercury Electrodes

Mercury is a very attractive choice for electrode materials because it has a high hydrogen overvoltage that greatly extends the cathodic potential window (compared to solid electrode materials) and possesses a highly reproducible, readily renewable, and smooth surface. In electrochemical terms, its roughness factor is equal to one (i.e., identical geometric and actual surface areas). Disadvantages of the use of mercury are its limited anodic range (due to the oxidation of mercury) and toxicity.

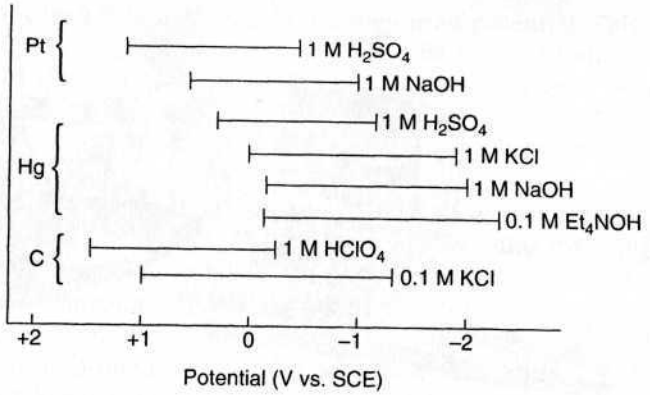

Figure 4.5 Accessible potential window of platinum, mercury, and carbon electrodes in various supporting electrolytes.

There are several types of mercury electrodes. Of these, the dropping mercury electrode (DME), the hanging mercury drop electrode (HMDE), and the mercury film electrode (MFE) are the most frequently used. Related solid amalgam electrodes have been introduced more recently to address concerns related to the toxicity of mercury.

The DME, used in polarography (Section 3.2) and for electrocapillary studies (Section 1.4), consists of a 12–20-cm-long glass capillary tubing (with an internal diameter of 30–50 μm), connected by a flexible tube to an elevated reservoir of mercury (Fig. 4.6). Electrical contact is effected through a wire inserted into the mercury reservoir. Mercury flows by gravity through the capillary at a steady rate, emerging from its tip as continuously growing drops. By adjusting the height of the mercury column, one may vary the drop time; the lifetime of the drop is typically 2–6 s. Such continuous exposure of fresh spherical drops eliminates passivation problems that may occur at stable solid electrodes. The key to successful operation of the DME is proper maintenance of its capillary (which prevents air bubbles, solution creeping, and dirt). More elaborate DMEs, based on a mechanical drop detachment at reproducible time intervals, are used for pulse polarography.

The hanging mercury drop electrode is a popular working electrode for stripping analysis and cyclic voltammetry. In this configuration, stationary mercury drops are displaced from a reservoir through a vertical capillary. Early (Kemula-type) HMDE designs rely on a mechanical extrusion (by a micrometer-driven syringe) from a reservoir through a capillary (13). The mercury reservoir should be completely filled with mercury; air must be fully eliminated. Modern HMDEs (particularly with the model 303 of EG&G PAR, shown in Fig. 4.7) employ an electronic control of the drop formation, which offers improved reproducibility and stability (14). For this purpose, a solenoid-activated valve dispenses the mercury rapidly, and the drop size is controlled

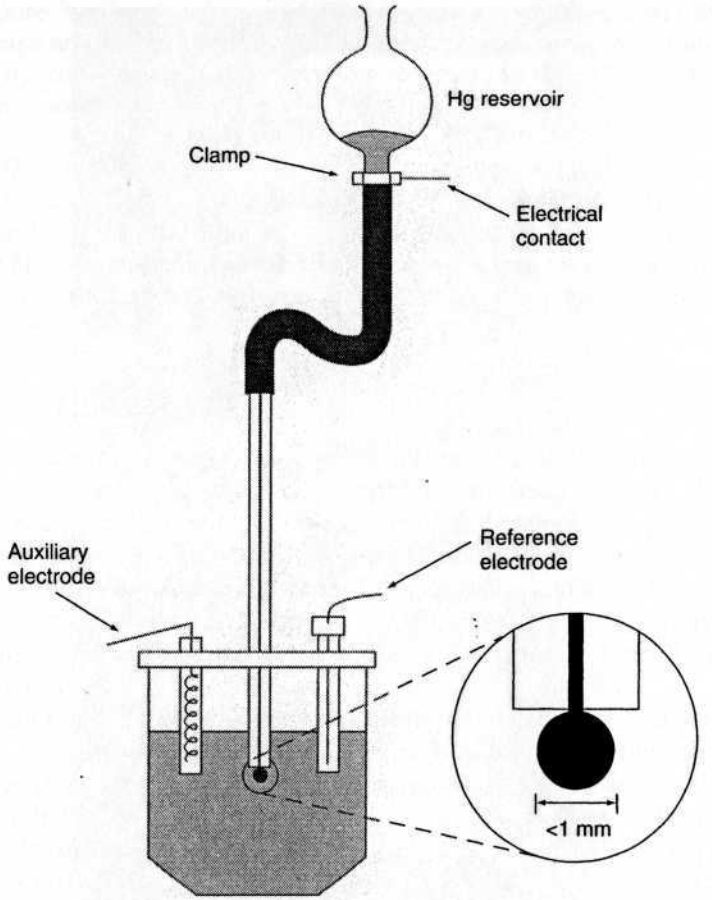

Figure 4.6 The dropping mercury electrode.

by the time during which the valve is opened. A wide-bore capillary allows a mercury drop to be grown very rapidly when the valve is opened. Three valve opening times produce drops that are described as small, medium, or large. Since the potential scan is accomplished after the valve has been closed (i.e., stationary electrode), charging-current contributions due to the drop growth are eliminated. All the components of this electrode, including the mercury reservoir, are contained in a compact unit. Such a commercial probe allows the conversion from the HMDE to DME by a single switch. When used in the DME mode, it exhibits a very rapid growth to a given area, which then remains constant (as desired for minimizing charging-current contributions). The performance of HMDEs can be improved by siliconizing the interior bore of the capillary.

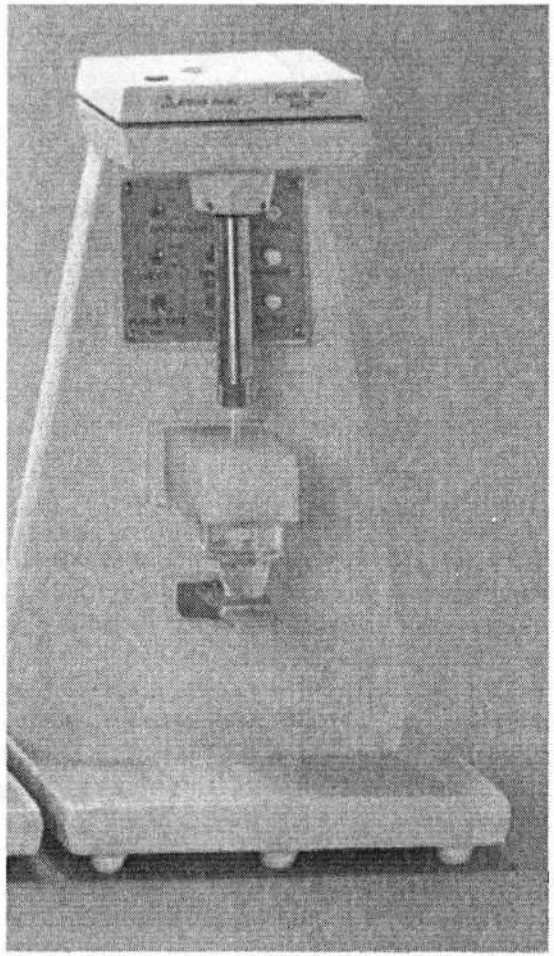

Figure 4.7 The static mercury drop electrode and its cell stand.

Several mercury electrodes combine the features of the DME and HMDE. In particular, one employs a narrow-bore capillary that produces DMEs with drop lifetimes of 50–70 s (15). The other involves a controlled growth mercury drop (16). For this purpose, a fast-response valve offers a wide range of drop sizes and a slowly (step-by-step) growing drop.

The mercury film electrode (MFE), used for stripping analysis or flow amperometry, consists of a very thin (10–100-μm) layer of mercury covering a conducting and inert support. Because of the adherent oxide films on metal surfaces, and the interaction of metals with mercury, glassy carbon is most often used as a substrate for the MFE. The mercury film formed on a glassy carbon support is actually composed of many droplets. Because they do not

have a pure mercury surface, such film electrodes exhibit a lower hydrogen overvoltage and higher background currents. Another useful substrate for the MFE is iridium (because of its very low solubility in mercury and the excellent adherence of the resulting film). Mercury film electrodes are commonly preplated by cathodic deposition from a mercuric nitrate solution. An in situ plated MFE is often employed during stripping analysis (17). This electrode is prepared by simultaneous deposition of the mercury and the measured metals. Most commonly, a disk-shaped carbon electrode is used to support the mercury film. Mercury film ultramicroelectrodes, based on coverage of carbon fiber or carbon microdisk surfaces, have also received a growing attention in recent years.

4.5.2 Solid Electrodes

The limited anodic potential range of mercury electrodes has precluded their utility for monitoring oxidizable compounds. Accordingly, solid electrodes with extended anodic potential windows have attracted considerable analytical interest. Of the many different solid materials that can be used as working electrodes, the most often used are carbon, platinum, and gold. Silver, nickel, and copper can also be used for specific applications. A monograph by Adams (18) is highly recommended for a detailed description of solid electrode electrochemistry.

An important factor in using solid electrodes is the dependence of the response on the surface state of the electrode. Accordingly, the use of such electrodes requires precise electrode pretreatment and polishing to obtain reproducible results. The nature of these pretreatment steps depends on the materials involved. Mechanical polishing (to a smooth finish) and potential cycling are commonly used for metal electrodes, while various chemical, electrochemical, or thermal surface procedures are added for activating carbon-based electrodes. Unlike mercury electrodes, solid electrodes present a heterogeneous surface with respect to electrochemical activity (19). Such surface heterogeneity leads to deviations from the behavior expected for homogeneous surfaces.

Solid electrodes can be stationary or rotating, usually in a planar disk configuration. Such electrodes consist of a short cylindrical rod of the electrode material embedded in a tightly fitting tube of an insulating material (Teflon, Kel-F, etc.). The construction of a typical disk electrode is illustrated in Figure 4.8. It is essential to use proper sealing to avoid crevices between the sleeve and the electrode materials, and thus to prevent solution creeping (and an increased background response). Electrical contact is made at the rear face. Disk solid electrodes are also widely employed in flow analysis in connection with thin-layer or wall-jet detectors (see Section 3.6). Other configurations of solid electrodes, including various ultramicroelectrodes (Section 4.5.4) and microfabricated screen-printed strips or silicon-based thin-film chips (Section 6.5), are attracting increasing attention.

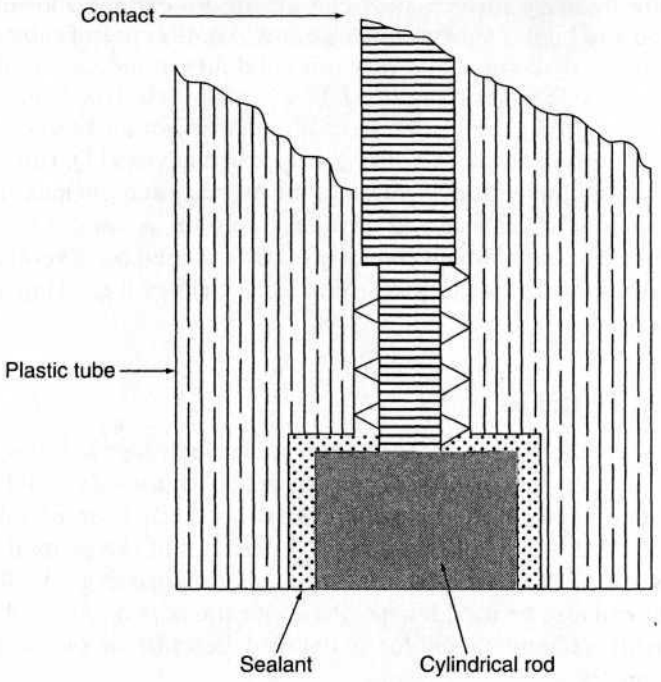

Figure 4.8 Construction of a typical disk electrode.

4.5.2.1 Rotating Disk and Rotating Ring Disk Electrodes The rotating disk electrode (RDE) is vertically mounted in the shaft of a synchronous controllable-speed motor and rotated with constant angular velocity (ω) about an axis perpendicular to the plain disk surface (Fig. 4.9a). [$\omega = 2\pi f$, where f is the rotation speed in rps (revolutions per second)]. As a result of this motion, the fluid in an adjacent layer develops a radial velocity that moves it away from the disk center. This fluid is replenished by a flow normal to the surface. Hence, the RDE can be viewed as a pump that draws a fresh solution up from the bulk solution. Under laminar flow conditions (usually up to ~4000 rpm), the thickness of the diffusion layer decreases with increasing electrode angular velocity according to

$$\delta = 1.61 D^{1/3} \omega^{-1/2} \nu^{1/6} \tag{4.4}$$

where ν is the kinematic viscosity (defined as the viscosity divided by the density in cm^2/s). Rotation speeds of 100–4000 rpm thus correspond to δ values in the 5–50 μm range. Equation (4.4) suggests that the thickness of the diffusion layer is independent of the disk diameter, namely, a uniform layer across the surface. The limiting current (for a reversible system) is thus proportional to the square root of the angular velocity, as described by the *Levich equation*:

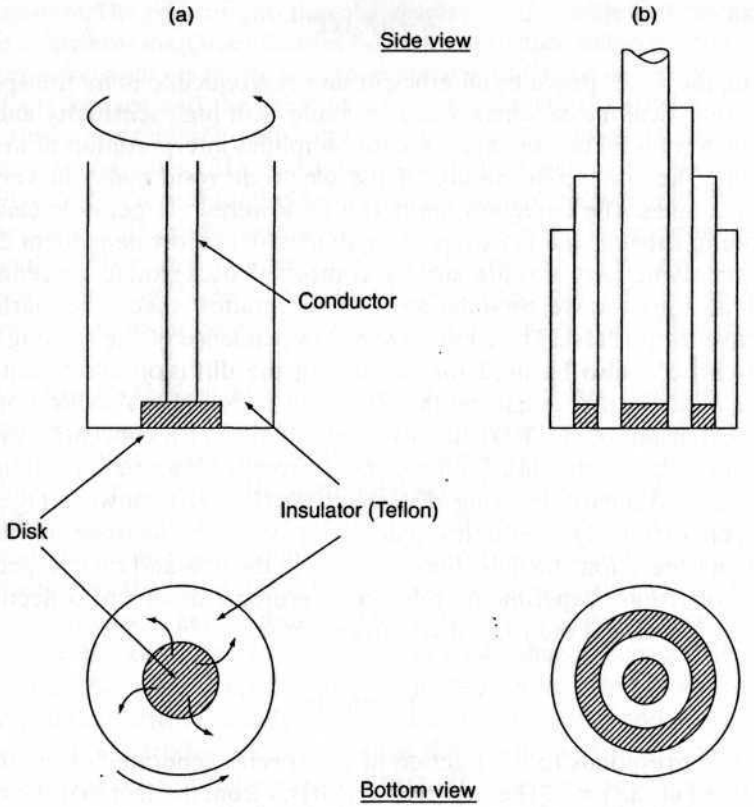

Figure 4.9 Rotating disk (a) and ring–disk (b) electrodes.

$$i_l = 0.62 n F A D^{2/3} \omega^{1/2} \nu^{-1/6} C \tag{4.5}$$

An increase in ω from 400 to 1600 rpm thus results in a twofold increase of the signal. A deviation from a linear plot of i_l vs. $\omega^{1/2}$ plot suggests some kinetic limitations. In addition, at very low rotation speeds (0–100 rpm), a slight upward bend is observed, due to contribution by natural convection. The voltammetric wave has a sigmoidal shape; for reversible systems it is identical to that common in DC polarography (described in Section 3.2), and independent of ω.

For quasi-reversible systems the limiting current is controlled by both mass transport and charge transfer:

$$i_l = nFADC\left(1/1.61 D^{1/3} \omega^{-1/2} \nu^{1/6} + k/D\right) \tag{4.6}$$

where k is the specific heterogeneous rate constant. In the limit of purely kinetically controlled process ($k < 10^{-6}$ m/s), the current becomes independent of the rotation speed:

$$i_l = nFAkC \tag{4.7}$$

Overall, the RDE provides an efficient and reproducible mass transport and hence analytical measurements can be made with high sensitivity and precision. Such well-defined behavior greatly simplifies interpretation of the measurement. The convective nature of the electrode results also in very short response times. The detection limits can be lowered via periodic changes in the rotation speed, and isolation of small mass-transport-dependent currents from simultaneously flowing surface-controlled background currents. Sinusoidal or square-wave modulations of the rotation speed are particularly attractive for this task. The rotation speed dependence of the limiting current [Eq. (4.5)] can also be used for calculating the diffusion coefficient or the surface area. Further details on the RDE can be found in Adams' book (18).

An extension of the RDE involves an addition of a concentric-ring electrode surrounding the disk (and separated from it by a small insulating gap) (20). The resulting rotating ring–disk electrode (RRDE), shown in Figure 4.9b, has been extremely useful for elucidating various electrode mechanisms (through generation and detection reactions at the disk and ring, respectively). Such "collection" experiments rely on measurements of the collection efficiency (N), which is the ring : disk current ratio:

$$N = -i_R / i_D \tag{4.8}$$

Here, N corresponds to the fraction of the species generated at the disk that is detected at the ring. (The negative sign arises from the fact that the currents pass in opposite directions.) Hence, the "collection" current is proportional to the "generation" current. Such experiments are particularly useful for detecting short-lived intermediate species (as the observed N values reflect the stability of such species). Analogous "collection" experiments can be carried out using dual-electrode flow detectors, described in Chapters 3–6.

4.5.2.2 Carbon Electrodes Solid electrodes based on carbon are currently in widespread use in electroanalysis, primarily because of their broad potential window, low background current, rich surface chemistry, low cost, chemical inertness, and suitability for various sensing and detection applications. In contrast, electron transfer rates observed at carbon surfaces are often slower than those observed at metal electrodes. Electron transfer reactivity is strongly affected by the origin and history of the carbon surface (21,22). Numerous studies have thus been devoted for understanding the structure–reactivity relationship at carbon electrodes (21). While all common carbon electrode materials share the basic structure of a six-member aromatic ring and sp^2 bonding, they differ in the relative density of the edge and basal planes at their surfaces. The edge orientation is more reactive than is the graphite basal plane toward electron transfer and adsorption. Materials with different edge-to-basal plane ratios thus display different electron transfer kinetics for a given

redox analyte. The edge orientation also displays undesirably high background current contributions. Other factors, besides the surface microstructure, affect the electrochemical reactivity at carbon electrodes. These include the cleanliness of the surface and the presence of surface functional groups. A variety of electrode pretreatment procedures have been proposed to increase the electron transfer rates (21). The type of carbon, as well as the pretreatment method, thus has a profound effect on the analytical performance. The most popular carbon electrode materials are those involving glassy carbon, carbon paste, carbon fiber, screen-printed carbon strips, carbon films, or other carbon composites (e.g., graphite epoxy, wax-impregnated graphite, Kelgraf). The properties of different types of carbon electrodes are discussed below.

4.5.2.2.1 Glassy Carbon Electrodes Glassy (or "vitreous") carbon has been very popular because of its excellent mechanical and electrical properties, wide potential window, chemical inertness (solvent resistance), and relatively reproducible performance. The material is prepared by means of a careful controlled heating program of a premodeled polymeric (phenolformaldehyde) resin body in an inert atmosphere (18). The carbonization process proceeds very slowly over the 300–1200°C temperature range to ensure the elimination of oxygen, nitrogen, and hydrogen. The structure of glassy carbon involves thin, tangled ribbons of cross-linked graphite-like sheets. Because of its high density and small pore size, no impregnating procedure is required. However, surface pretreatment is usually employed to create active and reproducible glassy carbon electrodes and to enhance their analytical performance (19). Such pretreatment is usually achieved by polishing (to a shiny "mirror-like" appearance) with successively smaller alumina particles (down to 0.05 μm). The electrode should then be rinsed with deionized water before use. Additional activation steps, such as electrochemical, chemical, heat, or laser treatments, have also been used to enhance the performance (21). The improved electron transfer capability has been attributed to the removal of surface contaminants, exposure of fresh carbon edges, and an increase in the density of surface oxygen groups (that act as interfacial surface mediators). Several reviews provide more information on the physical and electrochemical properties of glassy carbon electrodes (21,25).

A similar, but yet highly porous, vitreous carbon material, reticulated vitreous carbon (RVC), has found widespread applications for flow analysis and spectroelectrochemistry (26). As shown in Figure 4.10, RVC is an open-pore ("sponge-like") material; such a network combines the electrochemical properties of glassy carbon with many structural and hydrodynamic advantages. These include a very high surface area (~66 cm^2/cm^3 for the 100-ppi grade), 90–97% void volume, and a low resistance to fluid flow.

4.5.2.2.2 Carbon Paste Electrodes Carbon paste electrodes, which use graphite powder mixed with various water-immiscible nonconducting organic binders (pasting liquids), offer an easily renewable and modified surface, low

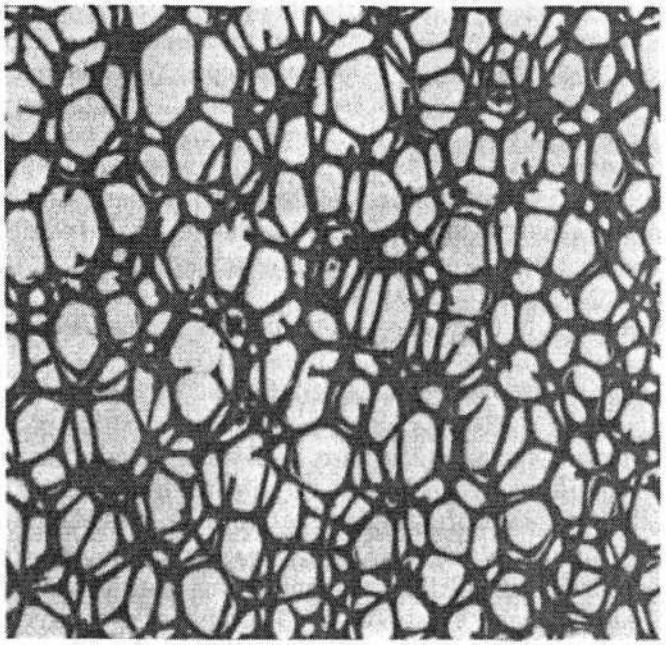

Figure 4.10 The open-pore structure of reticulated vitreous carbon.

cost, and very low background current contributions (27–29). A wide choice of pasting liquids is possible, but practical considerations of low volatility, purity, and economy narrow the choice to a few liquids. These include Nujol (mineral oil), paraffin oil, silicone grease, and bromonaphthalene. The former appears to perform the best. The paste composition strongly affects the electrode reactivity, with the increase in pasting liquid content decreasing the electron transfer rates, as well as the background current contributions (29). In the absence of pasting liquid, the dry graphite electrode yields very rapid electron transfer rates (approaching those of metallic surfaces). Despite their growing popularity, the exact behavior of carbon paste electrodes is not fully understood. It is possible that some of the electrochemistry observed at these electrodes involves permeation of the pasting liquid layer by the electroactive species (i.e., solvent extraction). Carbon paste represents a convenient matrix for the incorporation of appropriate modifying moieties (30). The modifier is simply mixed together with the graphite/binder paste (with no need to devise individualized attachment schemes for each modifier). Enzyme-containing carbon pastes have been used as rapidly responding reagentless biosensors (see Chapter 6). A disadvantage of carbon pastes is the tendency of the organic binder to dissolve in solutions containing an appreciable fraction of organic solvent. Two-dimensional carbon composite electrodes, based on the screen-printing technology, can be prepared from carbon inks consisting of graphite particles, a polymeric binder, and other additives (see Chapter 6).

4.5.2.2.3 Carbon Fiber Electrodes The growing interest in ultramicroelectrodes (Section 4.5.4) has led to a widespread use of carbon fibers in electroanalysis. Such materials are produced, mainly in the preparation of high-strength composites, by high-temperature pyrolysis of polymer textiles or via catalytic chemical vapor deposition. Different carbon fiber microstructures are available, depending on the manufacturing process. They can be classified into three broad categories: low-, medium-, and high-modulus types. The latter is most suitable for electrochemical studies because of its well-ordered graphite-like structure and low porosity (31). Improved electron transfer performance can be achieved by various electrode pretreatments, particularly "mild" and "strong" electrochemical activations, or heat treatment (32). Most electroanalytical applications rely on fibers of 5–20 μm diameter that provide the desired radial diffusion. Such fibers are typically mounted at the tip of a pulled glass capillary with epoxy adhesive, and are used in cylindrical or disk configurations. Precautions should be taken to avoid contamination of the carbon surface with the epoxy. The main advantage of carbon fiber microelectrodes is their small size (5–30 μm diameter of commercially available fibers) that makes them very attractive for anodic measurements in various microenvironments, such as the detection of neurotransmitter release in the extracellular space of the brain. Nanometer-size carbon fibers can be prepared by etching the fiber in flame or under ion beam (e.g., see Fig. 4.11). The various electroanalytical applications of carbon fibers have been reviewed by Edmonds (33).

4.5.2.2.4 Diamond Electrodes Although diamond itself is a known insulator, boron-doped diamond films possess electronic properties ranging from semiconducting to semimetallic and are highly useful for electrochemical measurements. For example, boron doping levels as high as 10^{21} cm^{-3} have been achieved, leading to resistivities lower than 0.01 Ω·cm. Boron-doped diamond (BDD) film electrodes, fabricated by chemical vapor deposition methods, have been studied intensely because of their attractive properties (34,35). These properties include a wide potential window (approaching 3 V, reflecting the high overvoltages for oxygen, chlorine, and hydrogen evolution), low and stable background currents (of a factor of ~10 less than comparably sized polished glassy carbon electrodes), favorable signal: background characteristics, negligible adsorption of organic compounds (i.e., resistance to fouling and a highly stable response), good electrochemical reactivity without any pretreatment, low sensitivity to dissolved oxygen, and extreme hardness. These very low background currents of BDD thin-film electrodes reflect their small double-layer capacitance values, such as 4–8 μF/cm^2 in 1 M KCl over a 2-V window, compared to 25–35 μF/cm^2 under similar conditions at glassy carbon electrodes. This is attributed, in part, to the absence of carbon–oxygen functionalities (35).

Diamond electrodes thus open up new opportunities for work under extreme conditions, including very high anodic potentials, surfactant-rich

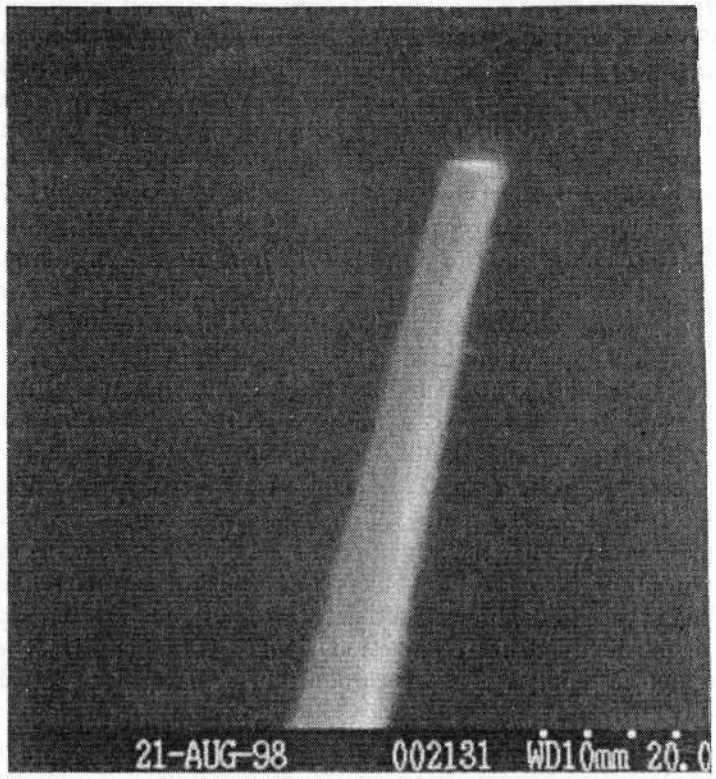

Figure 4.11 Scanning electron image of a carbon fiber electrode.

media, polarization in acidic media, or power ultrasound. Such capabilities and advantages have been illustrated for a wide range of electroanalytical applications, ranging from flow detection of chlorophenols (36) to direct electrochemistry of cytochrome C (37).

4.5.2.3 Metal Electrodes While a wide choice of noble metals is available, platinum and gold are the most widely used metallic electrodes. Such electrodes offer very favorable electron transfer kinetics and a large anodic potential range. In contrast, the low hydrogen overvoltage at these electrode limits the cathodic potential window (to the $-0.2 \rightarrow -0.5$-V region, depending on the pH). More severe are the high background currents associated with the formation of surface oxide or adsorbed hydrogen layers (e.g., see Fig. 4.12). Such films can also strongly alter the kinetics of the electrode reaction, leading to irreproducible data. These difficulties can be addressed with a pulse potential (cleaning–reactivation) cycle, as common in flow amperometry (39). The surface-layer problem is less severe in nonaqueous media, where noble metals

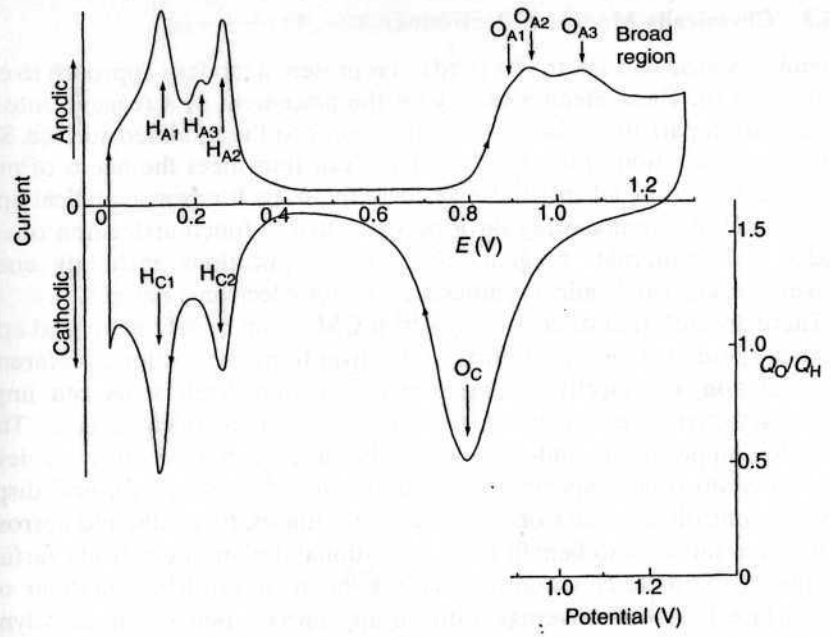

Figure 4.12 Current–potential curve for platinum surface oxide formation and reduction in 0.5 M H_2SO_4. (Reproduced with permission from Ref. 38.)

are often an ideal choice. Compared to platinum electrodes, gold ones are more inert, and hence are less prone to the formation of stable oxide films or surface contamination. Gold electrodes are also widely used as substrates for self-assembled organosulfur monolayers or for stripping measurements of trace metals (Sections 4.5.3 and 3.5; respectively).

Other metals, such as copper, nickel, or silver, have been used as electrode materials in connection with specific applications, such as the detection of amino acids or carbohydrates in alkaline media (copper and nickel) and cyanide or sulfur compounds (silver). Unlike platinum or gold electrodes, these electrodes offer a stable response for carbohydrates at constant potentials, through the formation of high-valence oxyhydroxide species formed in situ on the surface and believed to act as redox mediators (40,41). Bismuth film electrodes (preplated or in situ plated ones) have been shown to be an attractive alternative to mercury films used for stripping voltammetry of trace metals (42,43). Alloy electrodes (e.g., platinum–ruthenium, nickel–titanium) are also being used for addressing adsorption or corrosion effects of one of their components. The bifunctional catalytic mechanism of alloy electrodes (such as Pt–Ru or Pt–Sn ones) has been particularly useful for fuel cell applications (44).

4.5.3 Chemically Modified Electrodes

Chemically modified electrodes (CMEs) represent a modern approach to electrode systems. These electrodes rely on the placement of a reagent onto the surface, to impart the behavior of that reagent to the modified surface. Such deliberate alteration of electrode surfaces can thus meet the needs of many electroanalytical problems, and may form the basis for new analytical applications and different sensing devices. Such surface functionalization of electrodes with molecular reagents has other applications, including energy conversion, electrochemical synthesis, and microelectronic devices.

There are different directions by which CMEs can benefit analytical applications. These include acceleration of electron transfer reactions, preferential accumulation, or selective membrane permeation. Such steps can impart higher selectivity, sensitivity, or stability on electrochemical devices. These analytical applications and improvements have been extensively reviewed (45–47). Many other important applications, including electrochromic display devices, controlled release of drugs, electrosynthesis, fuel cells, and corrosion protection, should also benefit from the rational design of electrode surfaces.

One of the most common approaches for incorporating a modifier onto the surface has been coverage with an appropriate polymer film. Polymer-modified electrodes are often prepared by casting a solution droplet containing the dissolved polymer onto the surface and allowing the solvent to evaporate, by dip or spin coatings, or via electropolymerization in the presence of the dissolved monomer. The latter method offers precise control of the film thickness (and often the morphology), and is particularly attractive in connection with miniaturized sensor surfaces. The structure of some common polymeric coatings is shown in Figure 4.13. For example, the Dupont Nafion perfluorinated sulfonated cation exchanger (Fig. 4.13a) has been widely used as electrode modifier because of its attractive permselective, ion exchange, and antifouling properties (see examples below). In addition to diverse sensing applications, it has been widely used as a proton exchange membrane in fuel cells. Additional advantages can be attained by coupling two (or more) polymers in a mixed or multilayer configuration. Other useful modification schemes include bulk modification of composite carbon materials, covalent (chemical) attachment, sol-gel encapsulation, physical adsorption, and spontaneous chemisorption.

4.5.3.1 Self-Assembled Monolayers Spontaneously adsorbed monolayers of *n*-alkanethiols [$X(CH_2)_nSH$, with $n > 10$] on gold surfaces, based on the strong interaction between gold and sulfur, are particularly well suited for controlling and manipulating the reactivity at the interface. Such monolayers are commonly formed by immersing the gold electrode in ethanolic solutions containing millimolar concentrations of the alkanethiol overnight. The formation of self-assembled organosulfur monolayers (SAMs) has attracted considerable attention since the late 1980s because of its potential use in many scientific

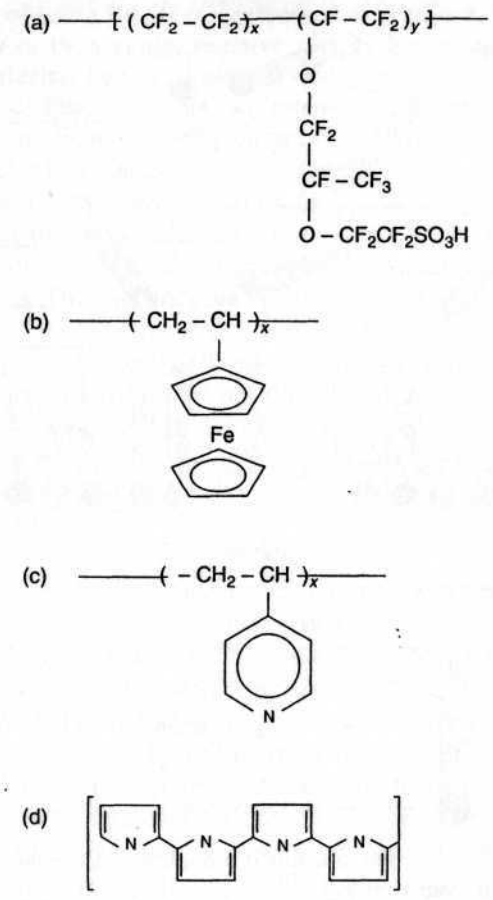

Figure 4.13 Structure of common polymeric coatings: (a) Nafion, (b) polyvinylferrocene; (c) polyvinylpyridine; (d) polypyrrole.

and technological applications (48–50). In addition to fundamental studies on the structure of such monolayers and long-range electron transfer, such applications include chemical sensors and biosensors, information storage devices, or lithography.

Cleavage of the S—H bond is central to this monolayer formation:

$$RSH + Au \rightleftharpoons RS\text{—}Au + e^- + H^+ \qquad (4.9)$$

Van der Waals forces between the methylene groups orient the monolayer. Such a self-assembly process thus results in well-organized and stable monolayers, with the hydrocarbon tails packed parallel to each other, tilted at ~30° relative to the surface normal (Fig. 4.14). The closely-packed pinhole-free films (surface coverage of $\sim 9 \times 10^{-10}$ mol/cm^2) block transport of species to the

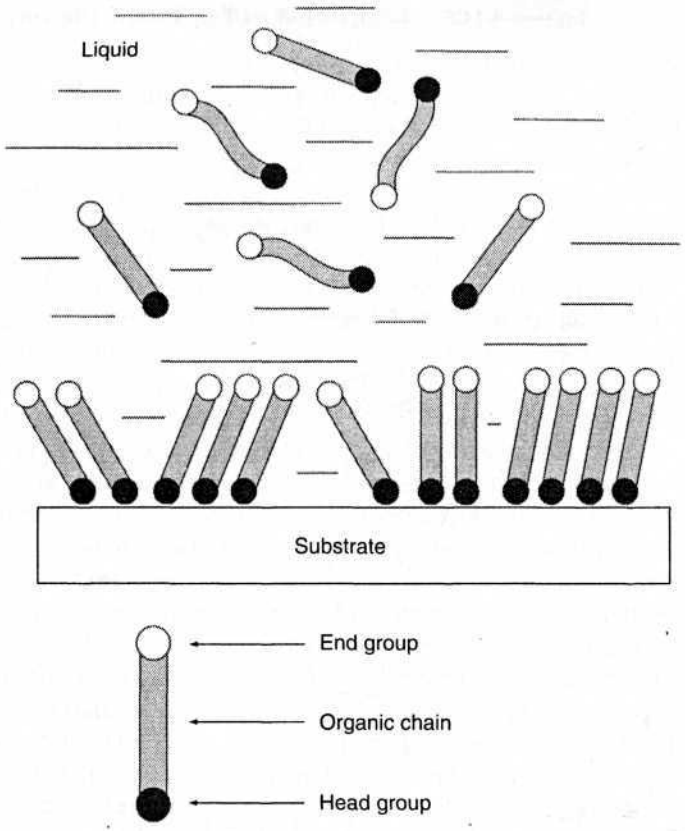

Figure 4.14 Formation of a self-assembled monolayer at a gold substrate. (Reproduced with permission from Ref. 48.)

underlying gold surface. The packing and order are influenced by factors such as chain length, end group, solvent, immersion time, or substrate morphology. Increasingly disordered structures with lower packing density and coverage are observed on decreasing the chain length ($n < 10$). These and other structural disorders and defects (e.g., pinholes) often lead to degraded performance. Coassembled monolayers, formed from mixtures of alkanethiols, can offer compositional and topographical variations in the film architecture. Differences in the coassembled two alkanethiols can be exploited for a selective removal of one component (e.g., by reductive desorption). Patterned SAM nanostructures can be prepared by an AFM-based "dip-pen" lithographic technique (51). Submicrometer SAM patterns can also be prepared by microcontact printing, involving transfer of a pattern from an elastomeric stamp to the gold surface (52). Alkanethiol monolayers can also be assembled on gold nanoparticles confined to carbon electrodes.

The novelty of using SAMs stems from their ability to be further modified into chemically or biologically reactive surface layers (via covalent coupling of different materials to the functional end group, X). Such use of SAM for anchoring various functionalities can impart specific interactions essential for various sensing applications (see Chapter 6). SAMs of DNA oligonucleotides on gold electrodes have been particularly useful for the development of DNA hybridization biosensors (see Section 6.1.2.2). These applications can benefit from the use of mixed SAMs (e.g., monolayers of thiol-derivatized single-stranded oligonucleotide and 6-mercapto-1-hexanol) that minimize steric/hindrance effects. The high degree of order of SAMs has also allowed the development of detailed structure–function relationships for various electron transfer processes. The well-defined surfaces of SAM-modified electrodes have also been extremely useful for studying electron transfer rates of proteins (53). As expected, the rate constants have been found to depend on the length of the spacer (i.e., the donor–acceptor distance). Other highly ordered films, such as those of alkyl siloxane, can be formed on metal oxide surfaces (particularly SiO_2).

4.5.3.2 Carbon-Nanotube-Modified Electrodes Carbon nanotubes (CNTs) represent an increasingly important group of nanomaterials with unique geometric, mechanical, electronic, and chemical properties (54). CNTs can be divided into single-wall carbon-nanotubes (SWCNT) and multiwall carbon nanotubes (MWCNTs). SWCNTs possess a cylindrical nanostructure (with a high aspect ratio), formed by rolling up a single graphite sheet into a tube. Multiwall CNTs consist of an array of such nanotubes that are concentrically nested like rings of a tree trunk. The unique properties of CNT make them also extremely attractive for the tasks of surface modification and electrochemical detection. More recent studies have demonstrated that CNT-modified electrodes can promote the electrochemical reactivity of important analytes and impart resistance against surface fouling (55). The electrocatalytic activity of CNT has been attributed to the presence of edge plane defects at their end caps (56). "Trees" of aligned CNT in the nanoforest, prepared by self-assembly (Fig. 4.15), can act as molecular wires to allow electrical communication between the underlying electrode and redox proteins (covalently attached to the ends of the SWNT) (57,58). Such efficient electron transfer to enzyme redox centers offers great promise for the design of amperometric biosensors (59).

4.5.3.3 Sol-gel Encapsulation of Reactive Species Another new and attractive route for tailoring electrode surfaces involves the low-temperature encapsulation of recognition species within sol-gel films (60,61). Such ceramic films are prepared by the hydrolysis of an alkoxide precursors, such as $Si(OCH_3)_4$, under acidic or basic condensation, followed by polycondensation of the hydroxylated monomer to form a three-dimensional interconnceted porous network. The resulting porous glass-like material can physically retain

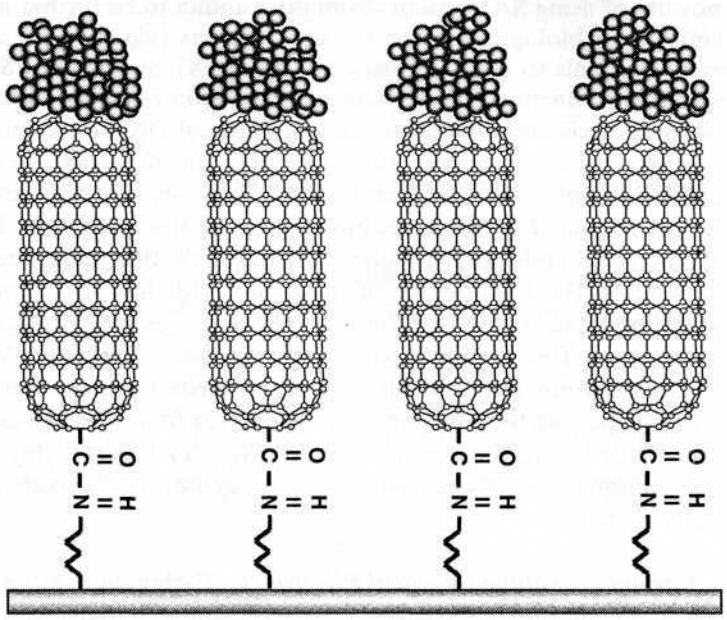

Figure 4.15 Nanoforest of vertically aligned CNT "trees" acting as molecular wires. (Reproduced with permission from Ref. 57.)

the desired modifier, but permits its interaction with the analyte that diffuses into the matrix. Besides their ability to entrap the modifier, sol-gel processes offer tunability of the physical characteristics (e.g., porosity), thermal stability, and mechanical rigidity. Sol-gel-derived composite electrodes have also been prepared by dispersing carbon or gold powders in the initial sol-gel mixture (62,63). Highly selective electrochemical sensors can be developed by application of molecular imprinting in sol-gel films, involving the formation of selective binding for the target analyte (64).

4.5.3.4 Electrocatalytically Modified Electrodes Often the desired redox reaction at the bare electrode involves slow electron transfer kinetics and therefore occurs at an appreciable rate only at potentials substantially higher than its thermodynamic redox potential. Such reactions can be catalyzed by attaching to the surface a suitable electron transfer mediator (65,66). Electrocatalytic reactions play a central role in electrochemistry and a vital role in sensing and energy-related applications. Knowledge of homogeneous solution kinetics is often used for selecting the surface-bound catalyst. The function of the mediator is to facilitate the charge transfer between the analyte and the electrode. In most cases the mediated reaction sequence (e.g., for a reduction process) can be described by

$$M_{ox} + ne^- \rightarrow M_{red} \quad (4.10)$$

$$M_{red} + A_{ox} \rightarrow M_{ox} + A_{red} \quad (4.11)$$

where M represents the mediator and A, the analyte. Hence, the electron transfer takes place between the electrode and mediator and not directly between the electrode and the analyte. The active form of the catalyst is electrochemically regenerated. The net results of this electron shuttling are a lowering of the overvoltage to the formal potential of the mediator and an increase in current density. The efficiency of the electrocatalytic process also depends on the actual distance between the bound redox site and the surface (since the electron transfer rate decreases exponentially when the electron–tunneling distance is increased).

The improvements in sensitivity and selectivity accrue from electrocatalytic CMEs have been illustrated for numerous analytical problems, including the biosensing of dihydronicotinamide adenine dinucleotide (NADH) at a Meldola Blue–coated electrode (67), the liquid chromatographic amperometric detection of thiols at cobalt phthalocyanine–coated electrodes (68), detection of nitric oxide release from a single cell by an electropolymerized nickel(II)-porphyrinic-based carbon fiber microsensor (69), flow injection measurements of carbohydrates at ruthenium dioxide–containing carbon paste detectors (70), and low-potential detection of hydrogen peroxide at Prussian Blue–modified electrodes (71). Cyclic voltammograms for various carbohydrates at the ruthenium dioxide carbon paste electrodes are shown in Figure 4.16. As expected for redox mediation, the peaks of the surface-bound ruthenium species (dashed lines) increase on addition of the carbohydrate analytes (solid lines). Figure 4.17 illustrates the electrocatalytic scheme involved in the detection of NADH. The implications of this scheme on various biosensors are discussed in Section 6.1. Electrocatalytic surfaces are also widely used in energy-producing fuel cells, particularly for catalyzing the oxidation of methanol or the reduction of oxygen (72).

4.5.3.5 Preconcentrating Electrodes Preconcentrating CMEs, with surfaces designed for reacting and binding of target analytes, hold great promise for chemical sensing (73–76). The concept is analogous to stripping voltammetric schemes, where the target analyte is preferentially partitioned from the dilute sample into the preconcentrating surface layer, and is subsequently reduced or oxidized during a potential scan. Unlike conventional stripping procedures, the preconcentration step is nonelectrolytic. Most preconcentrating CMEs employ electrostatic binding or coordination reactions, for collecting the analyte. Schemes based on hydrophobic partition into a lipid coating, covalent reactions, or peptide binding have also been reported. The preconcentrating agent may be incorporated within the interior of a carbon paste matrix or via functionalized polymeric and alkanethiol films. For example, as shown in Figure 4.18, ligand centers can covalently bind to a polymer back-

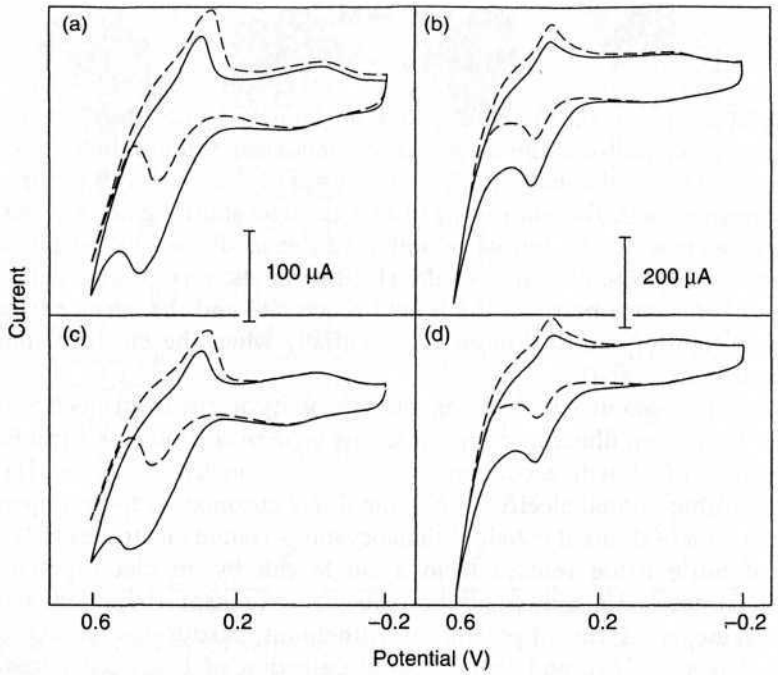

Figure 4.16 Cyclic voltammograms for 1.5×10^{-3} M ribose (a), glucose (b), galactose (c), and fructose (d) recorded at a RuO_2-modified carbon paste electrode. Dotted lines were obtained in carbohydrate-free solutions. (Reproduced with permission from Ref. 70.)

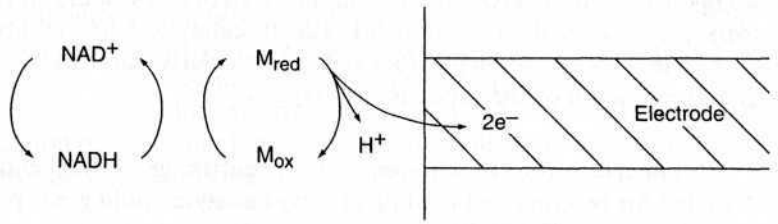

Figure 4.17 Electrocatalytic detection of NADH.

bone on the electrode to effectively accumulate and measure target metals. The major requirements for a successful analytical use of preconcentrating electrodes are strong and selective binding, prevention of saturation, and a convenient surface regeneration. Following the accumulation, the electrode can be transferred to more suitable solutions that facilitate the measurement and "cleaning" steps.

Practical examples of using preconcentrating CMEs include the use of a mixed 2,9-dimethyl-1,10-phenanthroline/carbon paste electrode for trace

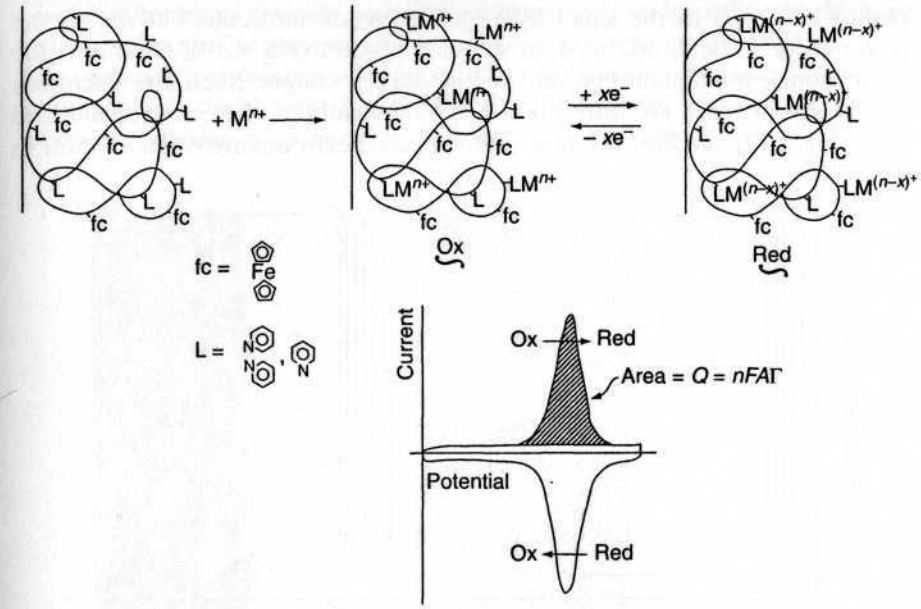

Figure 4.18 Preconcentrating surfaces based on covalent binding of the ligand to a polymer backbone. (Reproduced with permission from Ref. 74.)

measurements of copper (77), the use of clay-containing carbon pastes for voltammetric measurements of iron (78), the use of polyelectrolyte coatings for the uptake and voltammetry of multiple-charged metal complexes (79,80), the use of surface-bound crown ethers and cryptands for trace measurements of lead (81), the ion exchange voltammetric measurements of lanthanide ions at a Nafion-coated electrode (82), the collection of ultratrace cadmium onto mercaptocarboxylic acid monolayers (83), ultrasensitive biomimetric detection of copper based on a selective surface-confined peptide ligand (84), and the quantitation of nickel at porphyrin-coated electrodes (85).

4.5.3.6 Permselective Coatings Permselective coatings offer the promise of bringing higher selectivity and stability to electrochemical devices. This is accomplished by exclusion from the surface of unwanted matrix constituents, while allowing transport of the target analyte. Different avenues to control the access to the surface, based on different transport mechanisms, have been proposed. These include the use of size-exclusion poly(1,2-diaminobenzene) films (86), charged-exclusion ionomeric Nafion coatings (87), hydrophobic lipid (88) or alkanethiol (89) layers, or bifunctional (mixed) coatings (90). Such anti-interference membrane barriers offer an effective separation step (in situ on the surface), and hence protect the surface against adsorption of large macromolecules or minimize overlapping signals from undesired electroactive interferences. For example, the poly(1,2-diaminobenzene)-coated flow detector

rapidly responds to the small hydrogen peroxide molecule, but not to the larger ascorbic acid, uric acid, or cysteine species (Fig. 4.19). Note also the protection from foulants present in the serum sample. Such size exclusion (sieving) properties are attributed to the morphology of electropolymerized films (Fig. 4.20). Similarly, Nafion-coated microelectrodes are often used for in

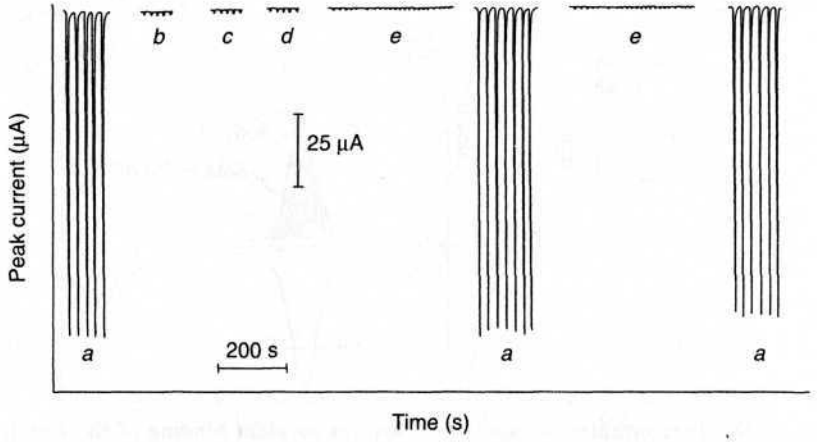

Figure 4.19 Permselective coatings: flow injection response of a poly (1,2-diaminobenzene)-coated electrode to the following: *a*, hydrogen peroxide (1 mM); *b*, ascorbic acid (1 mM); *c*, uric acid (1 mM); *d*, L-cysteine (1 mM); *e*, control human serum. (Reproduced with permission from Ref. 86.)

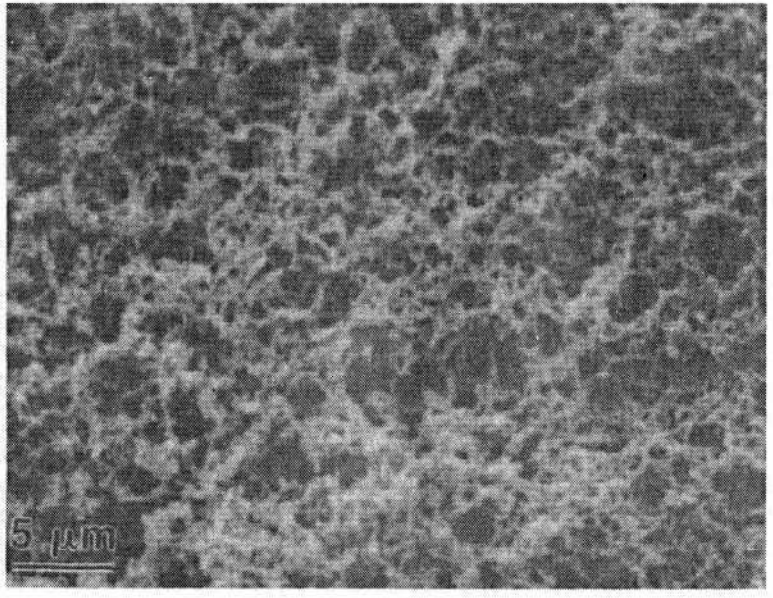

Figure 4.20 Scanning electron micrograph of a polyaniline-coated electrode.

vivo monitoring of cationic neurotransmitters, such as dopamine, in the brain extracellular fluid in the presence of otherwise interfering ascorbic acid (87). Such anionic interference is excluded from the surface through electrostatic repulsion with the negatively charged sulfonated groups (Fig. 4.21). Examples of these and other discriminative films are given in Table 4.2.

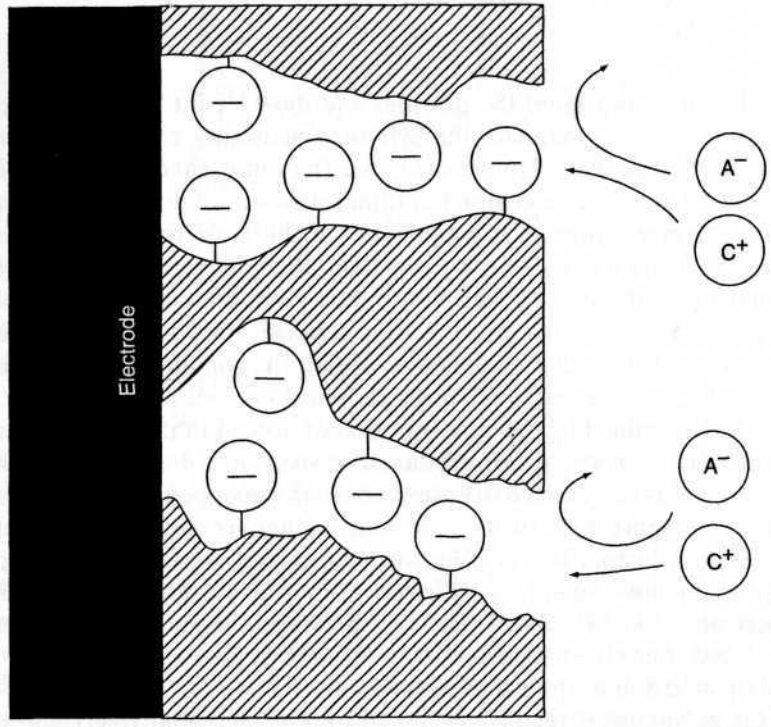

Figure 4.21 Use of negatively charged polymeric films for excluding anionic interferences.

TABLE 4.2 Commonly Used Membrane Barriers

Transport Mechanism	Membrane Barrier	Ref.
Size exclusion	Cellulose acetate	91
	Poly(1,2-diaminobenzene)	86
	Polyphenol	92
Hydrophobic barriers	Phospholipid	88
	Self-assembled thiols	89
Charge exclusion	Nafion	87
	Poly(ester sulfonic acid)	93
	Self-assembled thioctic acid	94
Mixed control	Cellulose acetate/Nafion	90

4.5.3.7 Conducting Polymers Electronically conducting polymers (such as polypyrrole, polythiophene, and polyaniline) have attracted considerable attention because of their ability to reversibly switch between the positively charged conductive state and a neutral, essentially insulating form, and to incorporate and expel anionic species (from and to the surrounding solution), on oxidation or reduction:

$$P^0 + A^- \rightarrow P^+A^- + e^- \qquad (4.12)$$

where P and A^- represent the polymer and the "dopant" anion, respectively. The latter serves to maintain the electrical neutrality, counterbalancing the positive charge of the polymer backbone. The redox changes [Eq. (4.12)] are not localized at a specific center, but rather delocalized over a number of conducting polymer groups. The conjugation of the π-electron system creates a molecular orbital which extends throughout the polymer chain. The electrical conductivity of these films, which originates from the electronic structure of their polymeric backbone (i.e., electron hopping involving the delocalized π electrons) can vary with the applied potential. The conductivity values depend on the amount of carriers (electrons or holes) created in the polymer chain (which is determined by the concentration of dopant in the polymer) and the carrier mobility through the polymer. The structure of common conducting polymers, and their conductivity range (from the undoped to doped states) are displayed in Figure 4.22. Such conductivity values are similar to those of inorganic semiconductors. It is possible also to use large organic anions (and even DNA) as dopants. Such large dopants cannot be readily expelled from the polymer network. As a result, when the polymeric chain becomes neutral (in the reduced state) the negative charge of the entrapped anionic dopant is balanced by insertion of the electrolyte cation.

These polymers are readily prepared by in situ electropolymerization (from the monomer solution). Oxidation of the monomer proceeds according to

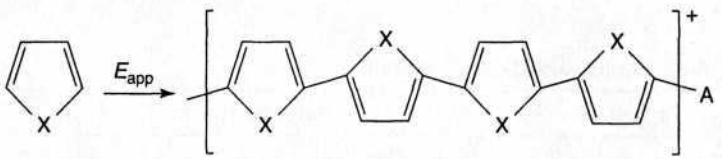

(4.13)

X = NH (polypyrrole)
X = S (polythiophene)
X = O (polyfuran)

Often the first step in the electropolymerization process is the electrooxidative formation of a radical cation from the starting monomer. This step is commonly followed by a dimerization process, followed by further oxidation and coupling reactions. Well-adhered films can thus be formed on the surface in galvanostatic, potentiostatic, or multiscan experiments. The behavior of elec-

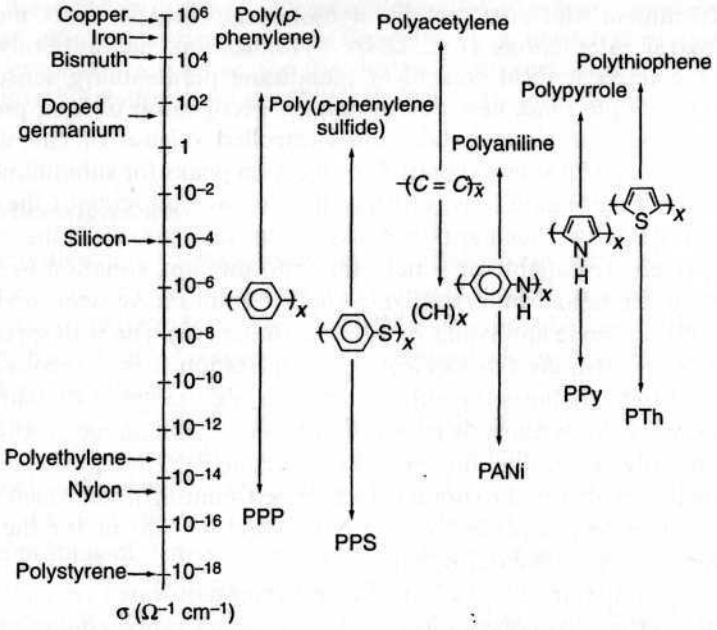

Figure 4.22 Conductivity ranges of common conducting polymers, along with their chemical structures. (Reproduced with permission from Ref. 95.)

tropolymerized films can be controlled by the polymerization conditions, including the electrolyte (particularly the nature and level of the anion serving as the dopant), solvent, monomer concentration, applied potential or current, and duration. The dynamic of the redox switching reaction [Eq. (4.12)] strongly depends on the ionic fluxes that accompany the process. As was discussed earlier, the tight entrapment of large anionic dopants (e.g., polyelectrolytes) precludes their removal, and hence the charge compensation is dominated by the movement of a "pseudodopant" cation.

Changes in the polymer properties can be induced by attaching various chemical or biological functionalities to the monomer prior to polymerization. A large variety of functions can thus be incorporated into conducting polymers owing to the richness of chemical synthesis. It is also possible to impart molecular recognition or electrocatalytic action via the incorporation of functional dopants (e.g., complexing agents or an electron transfer mediator). Hence, conducting polymers can act as efficient molecular interfaces between recognition elements and electrode transducers. The unique physical and chemical properties of conducting polymers, particularly the controllable and dramatic change in electrical conductivity and rapid exchange of the doping ion, offer diverse electrochemical applications, including batteries, fuel cells, corrosion protection, or chemical sensing (96). The latter include amperometric flow detection of nonelectroactive ions, solid-state gas sensing, entrap-

ment/attachment and stabilization of biological entities, direct monitoring of biological interactions (e.g., DNA hybridization and antibody–antigen binding), electrochemical control of membrane permeability, sensor arrays based on multiple films, new potentiometric recognition of ions, preconcentration/stripping of trace metals, and controlled release of chemicals. For example, Figure 4.23 shows typical flow injection peaks for submillimolar concentrations of carbonate ions (utilizing the doping-updoping of the polypyrrole-based detector). Such anodic peaks reflect the passage of the carbonate anions [which are capable of penetrating into the film, equation (4-12)] over the surface. These and other analytical opportunities have been reviewed by Ivaska (98), Teasdale and Wallace (99), and Bidan (95). The widespread use of polypyrrole is attributed to its electropolymerization from aqueous media at neutral pH (which allows the entrapment of a wide range of dopants). Other films are more limited in this regard. For example, thiophene is soluble only in organic solvents and aniline, only in acidic media. The electropolymerization growth can also lead to nonconducting, self-limiting films, which are often used as permselective/protective layers (Section 4.5.3.5) or for the physical entrapment of biomolecules (Chapter 6).

More recently introduced conducting polymer nanowires are characterized by higher surface : volume ratio (i.e., larger aspect ratio) compared to conventional conducting polymer films, and hence offer greater promise for resistive sensors and molecular electronic devices (100). Such scaling down of conducting polymer films into nanometer-scale wires leads to highly sensitive fast-responding sensors. Conducting polymer nanowires of controlled dimension can be readily prepared by a template-directed electrochemical synthesis involving electrodeposition into the pores of a membrane template or within the microchannels contacting neighboring microelectrodes (101,102).

Electropolymerization can also be used for the design of molecularly imprinted polymers (MIPs), capable of interacting with the analyte (template) molecule with high affinity and specificity (103,104). This is accomplished by electropolymerizing polypyrrole, polyaniline, or poly(*o*-phenylenediamine) in the presence of the analyte (template) molecule. At the end of the polymer-

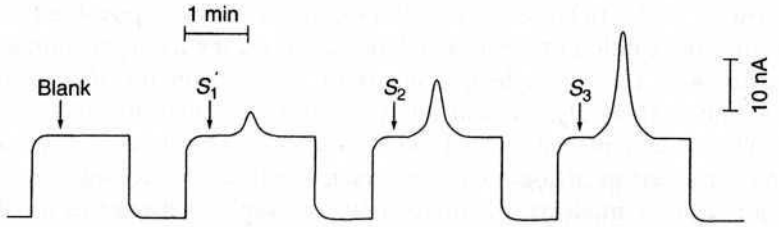

Figure 4.23 Typical response of polypyrrole detector to carbonate: S_1, 1×10^{-4} M; S_2, 2.5×10^{-4} M; S_3, 5×10^{-4} M, based on the doping–undoping process. (Reproduced with permission from Ref. 97.)

ization, the template is removed leaving a crosslinked polymer, containing sites with high affinity for the template (Fig. 4.24). Such electrical preparation of MIP is extremely attractive for the design of sensors with high molecular recognition capability. More details on MIP-based electrochemical sensors are given in Chapter 6.

4.5.4 Microelectrodes

Miniaturization is a growing trend in the field of analytical chemistry. The miniaturization of working electrodes not only has obvious practical advantages but also creates some fundamentally new possibilities (105–108). The term "microelectrodes" is reserved here for electrodes with at least one dimension not greater than 25 μm.

Such dimensions offer obvious analytical advantages, including the exploration of microscopic domains, measurements of local concentration profiles, detection in microflow systems, and analysis of very small (microliter) sample volumes. Particularly fascinating are more recent studies aimed at time-resolved probing of dynamic processes (e.g., secretion of chemical messengers) in single cells (109), the in vivo monitoring of neurochemical events (e.g., stimulated dopamine release) (110), the in vivo detection of nitric oxide (111), use of nanoscopic electrode tips for single-molecule detection (112), or high-resolution spatial characterization of surfaces (see Section 2-3). Figure 4.25 illustrates the use of a carbon fiber microelectrode for measuring the vesicular release of dopamine following cellular stimulation. Microelectrodes with 1 μm diameters provide spatial resolution sufficient to identify the locations of release sites on the surface of single cells (110).

Microelectrodes exhibit several other attractive and important properties that have expanded the possibilities of electrochemistry:

1. Because of the very small total currents at microelectrodes, it is possible to work in highly resistive solutions that would develop large ohmic (iR) drops

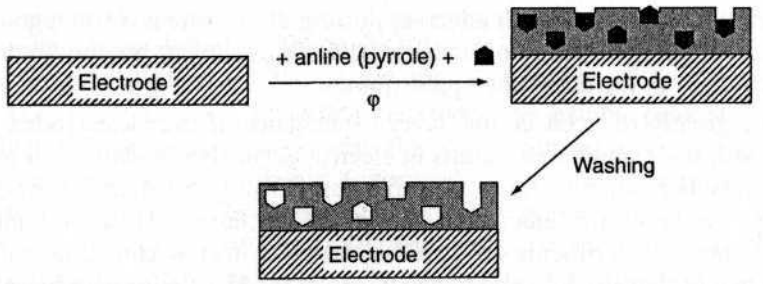

Figure 4.24 Use of electropolymerization from preparing molecularly imprinted polymers with sites with high affinity for the template (analyte) molecule. (Reproduced with permission from Ref. 103.)

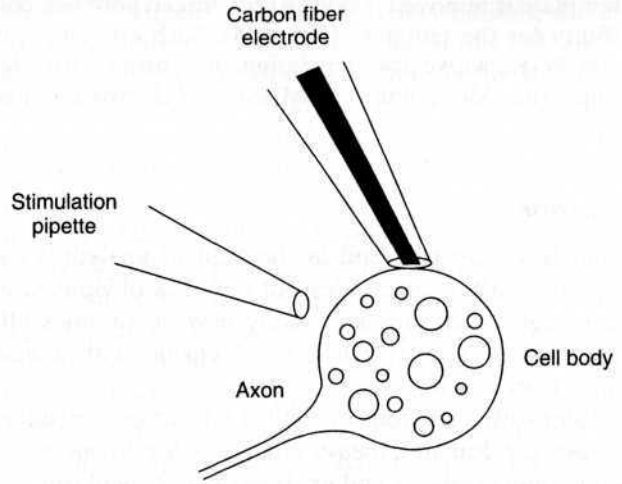

Figure 4.25 Experimental setup for monitoring dopamine release by exocytosis, from a cell body. The microelectrode and glass capillary (containing the chemical stimulant) are micromanipulated up to the cell body. (Reproduced with permission from Ref. 113.)

with conventional electrodes. The decreased ohmic distortions allow electrochemical measurements to be made on new and unique chemical environments (which are not amenable to macroscopic electrodes). Microelectrode experiments have thus been reported in low dielectric solvents (e.g., benzene, toluene), frozen acetonitrile, low-temperature glasses, gaseous and solid phases, supercritical carbon dioxide, ionically conductive polymers, oil-based lubricants, and milk. In addition, more traditional systems can be studied with little or no deliberately added supporting electrolyte, and with two-electrode systems. The use of electrolyte-free organic media can greatly extend the electrochemical potential window, thus allowing studies of species with very high oxidation potentials. Acetonitrile, for example, can be used to about 4 V (vs. a silver reference electrode), making possible studies of short-chain alkanes. Work without deliberately added supporting electrolyte is advantageous also for stripping voltammetry of trace metals as it minimizes potential impurities and changes in the chemical equilibrium.

2. The greatly reduced double-layer capacitance of microelectrodes, associated with their small area, results in electrochemical cells with small RC time constants. For example, for a microdisk the RC time constant is proportional to the radius of the electrode. The small RC constants allow high-speed voltammetric experiments to be performed at the microsecond timescale (scan rates higher than 10^6 V/s) and hence to probe the kinetics of very fast electron transfer and coupling chemical reactions (114) or the dynamic of processes such as exocytosis (e.g., Fig. 4.25). Such high-speed experiments are discussed further in Section 2.1.

3. Enhanced rates of mass transport of electroactive species accrue from the radial (nonplanar) diffusion to the edges of microelectrodes. Such "edge effects" contribute significantly to the overall diffusion current. The rate of mass transport to and from the electrode (and hence the current density) increases as the electrode size decreases. As a consequence of the increase in mass transport rates and the reduced charging currents, microelectrodes exhibit excellent signal-to-background characteristics in comparison to their large counterparts. In addition, steady-state or quasi-steady-state currents are rapidly attained, and the contribution of convective transport is negligible. The fact that redox reactions that are limited by mass transport at macroscopic electrodes become limited by the rate of electron transfer can also benefit many kinetic studies (115).

4.5.4.1 Diffusion at Microelectrodes The total diffusion-limited current is composed of the planar flux and radial flux diffusion components:

$$i_{\text{total}} = i_{\text{planar}} + i_{\text{radial}} \tag{4.14}$$

For disk, spherical, and hemispherical geometries, the general expression for the radial component in Eq. (4.14) is given by

$$i_{\text{radial}} = a r n F D C \tag{4.15}$$

where r is the electrode radius and a is a function of the electrode geometry. For disks, spheres, and hemispheres the a values are equal to 4, 4π, and 2π, respectively. Such radial diffusion leads to a larger flux at the perimeter of the electrode (than at the center), and hence to a nonuniform current density.

The extent by which the planar or radial component dominates depends on the relative dimensions of the electrode and the diffusion layer, as expressed by the dimensionless parameter Dt/r_0^2, where t is the electrolysis time, and r_0 is the smallest dimension of the electrode (116). For large (>1) values of Dt/r_0^2 (i.e., diffusion-layer thickness that exceeds the size of the electrode), the current approaches steady state, and sigmoidal voltammograms are observed. In contrast, planar diffusion dominates at small values of Dt/r_0^2, and a peak-shaped behavior is observed. Hence, depending on the timescale of the experiment (i.e., the scan rate), the same electrode may exhibit peak-shaped or sigmoidal voltammograms (e.g., see Fig. 4.26). Similarly, in the case of chronoamperometric experiments, a modified Cottrell equation predicts that a steady-state current is reached rapidly after the potential step (e.g., within ~10 ms and 1.3 s for 1- and 10-μm-diameter disks, respectively). The change from semiinfinite planar diffusion into semiinfinite hemispherical diffusion, associated with the decrease in the electrode dimension, is illustrated in Figure 4.27, which displays computed concentration profiles for a given time after the start of a chronoamperometric experiment at a disk with different radii.

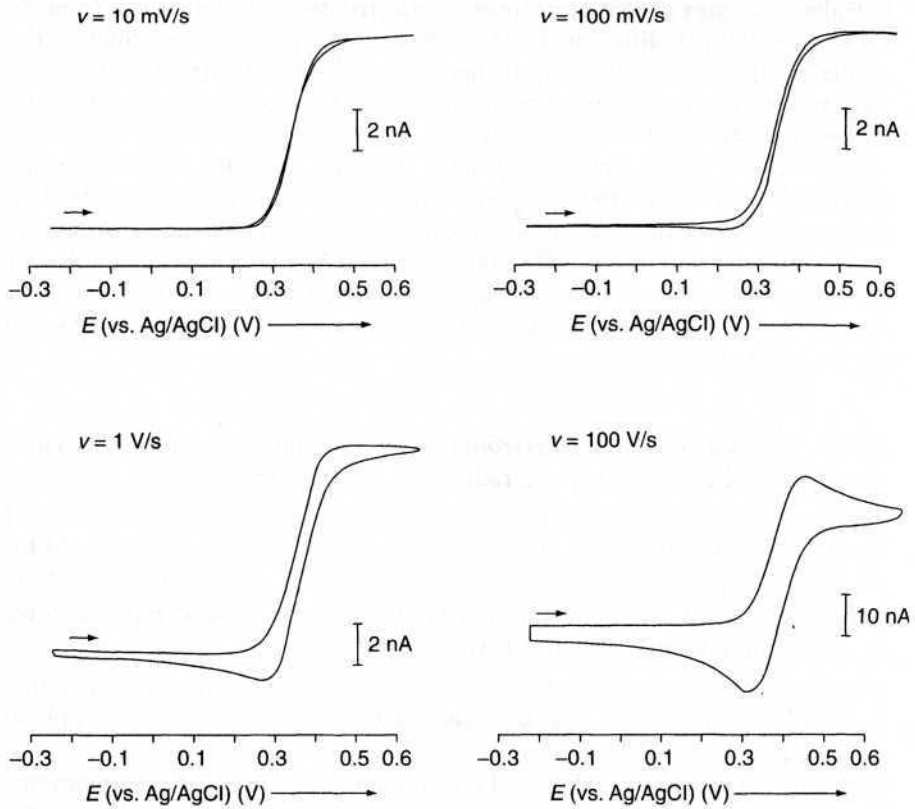

Figure 4.26 Cyclic voltammograms for the oxidation of ferrocene at a 6-μm platinum microdisk at different scan rates. (Reproduced with permission from Ref. 116.)

4.5.4.2 Microelectrode Configurations Electrodes of different materials have been miniaturized in many geometric shapes (Fig. 4.28), with the common characteristic that the electrode dimension is significantly smaller than the diffusion layer at the electrode surface (for ordinary voltammetric time scales, e.g., 1–10 s). The most commonly used shape is a circular conductor (of around 10 μm diameter), embedded in an insulating plane (the so-called microdisk electrode) (Fig. 4.28a). Other common geometries include the microring (Fig. 4.28b), microcylinder (Fig. 4.28c), microhemisphere (Fig. 4.28d), or microband (Fig. 4.28e) electrodes. Cylinder and band (line) microelectrodes, which can be several millimeters long, yield larger (and hence more easily measured) currents, while maintaining an enhanced diffusional flux. Band electrodes of nanoscopic dimensions can be fabricated by sealing ("sandwiching") ultrathin carbon and metal films between insulating supports and polishing one end of the sandwich or via photolithographic deposition of a thin metal film on an insulating substrate. The fabrication of most

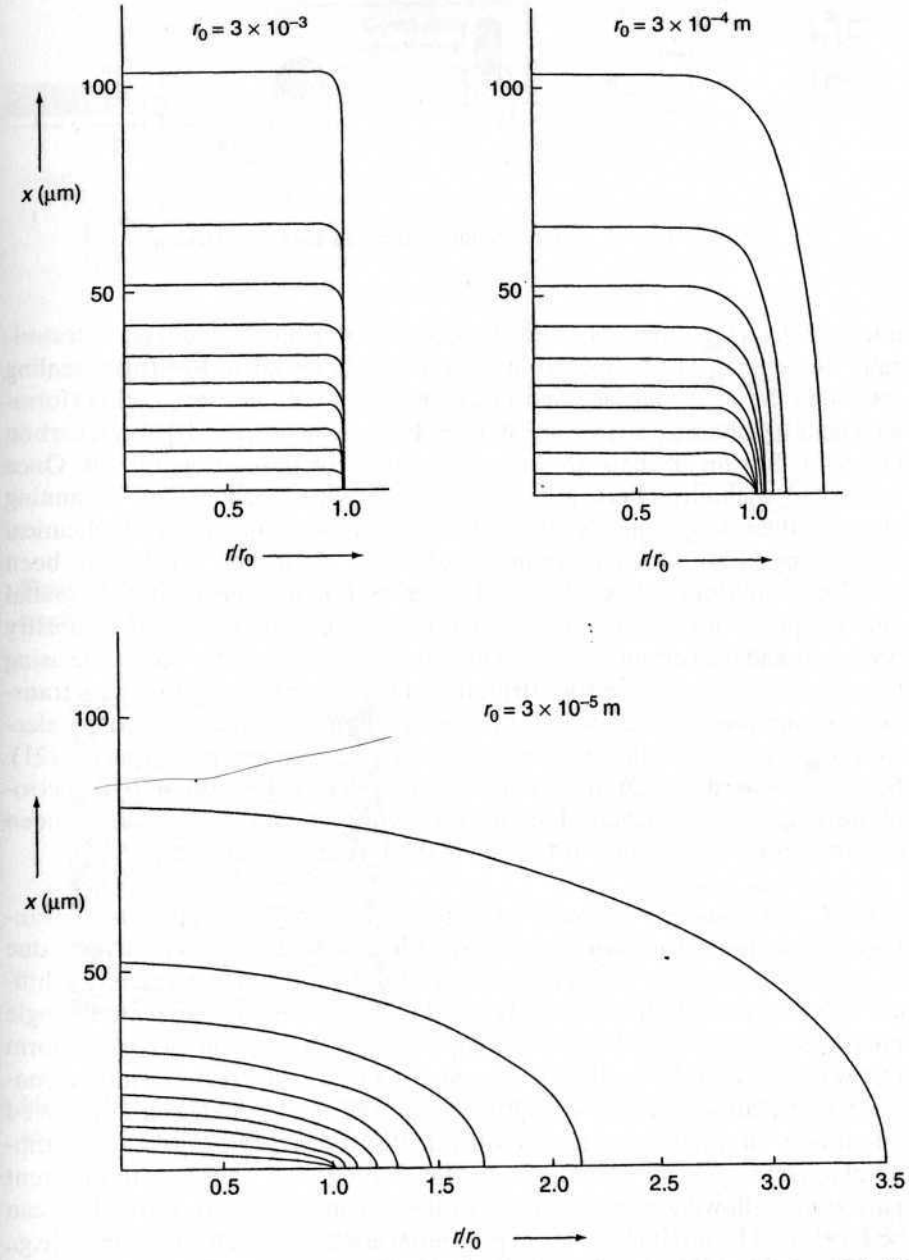

Figure 4.27 Normalized calculated concentration profiles for disk electrodes with different radii (r_0), 1 s after start of a chronoamperometric experiment. (Reproduced with permission from Ref. 116.)

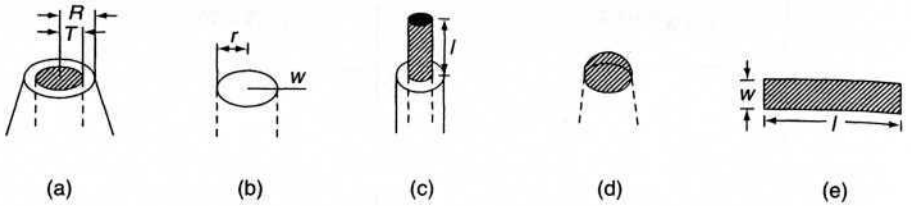

Figure 4.28 Common configurations of microelectrodes.

microelectrode geometries (with the exception of microcylinders) is technically demanding (108). Special attention should be given to proper sealing (between the active surface and insulating sheath) to ensure good performance and to minimize stray capacitances. Fine metal (Pt, Au, Ir) wires, carbon fibers, or thin metal films are commonly used for these preparations. Once fabricated, such ultramicroelectrodes are generally characterized by scanning electron microscopy, steady-state voltammetry, or scanning electrochemical microscopy (108). Molecule (nanometer)-sized electrodes, which have been developed in several laboratories (117–120), should offer additional spatial and temporal advantages, including a closer look at interfacial chemistry processes and measurements of fast electron transfer rates not accessible using larger microelectrodes. This is attributed to the very rapid rates of mass transport at nanoscale electrodes. The construction of such nanoscopic electrodes is even more challenging than their microscopic counterparts (121). Nanometer-sized (2–150-nm) platinum electrodes, fabricated by electrophoretic coating of etched platinum wire with poly(acrylic acid), have been shown useful for detecting as few as 7000 molecules (118).

4.5.4.3 Composite Electrodes Composite electrodes couple the advantages of single-microelectrode systems with significantly higher currents due to larger surface areas (122). Such electrodes thus address instrumental difficulties of monitoring the extremely small (subnanoampere) currents at single microelectrodes. The surface of composite electrodes consists of uniform (array) or random (ensemble) dispersion of a conductor region within a continuous insulating matrix (Fig. 4.29). Examples of arrays include closely spaced microdisks or interdigitated microband electrodes (e.g., Fig. 4.30). Lithographic techniques are often used for fabricating such arrays (with different patterning) allowing precise control of the spacing (123,124). Ensembles can be fabricated by mixing/pressing a powdered conductor with an insulator [e.g., Kel-F/graphite (125)], by impregnation of a porous conductor with an insulator [e.g., microcellular carbon/epoxy (126)], embedding carbon fibers in an insulating epoxy (127), or via deposition of a metal conductor into the pores of a microporous host membrane (101,128). The latter also represents an attractive route for preparing nanowires for a wide range of nanotechnology applications (in connection to dissolution of the membrane template) (129).

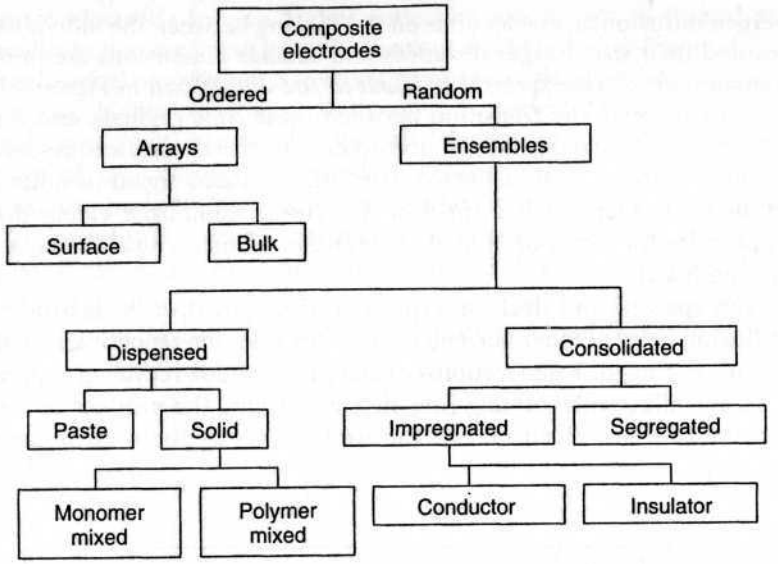

Figure 4.29 Classification of composite electrodes used in controlled-potential electrochemical techniques. (Reproduced with permission from Ref. 122.)

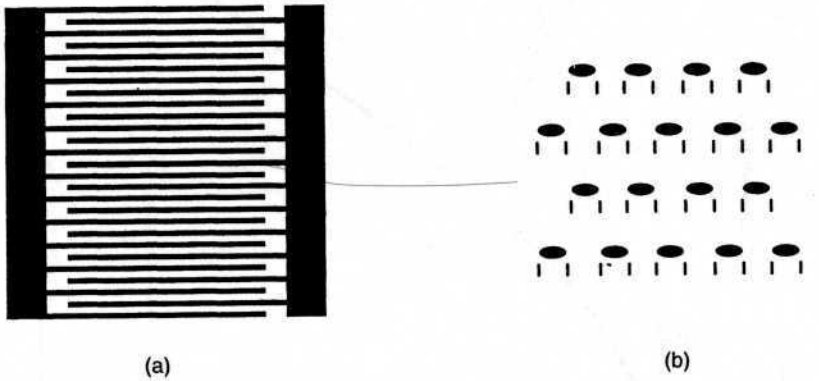

Figure 4.30 Schematic representation of an interdigitated microarray electrode (a) and closely spaced microdisk electrodes (b).

As long as there is a negligible overlap of the diffusion layers from adjacent sites (i.e., each member maintains its own radial diffusional field), the current of composite electrodes is the sum of currents of the individual sites. At sufficiently long times, the diffusion layers overlap, and the electrode behaves as though its entire geometric surface were active. For example, a slow scanning cyclic voltammetric experiment displays a current peak proportional to the total geometric area. The exact timescale for the change from isolated

to merged diffusion layers depends on the spacing between the individual electrodes and their size. Larger distances and smaller dimensions are preferred. Chronoamperometric experiments, such as the one shown in Figure 4.31, can be used to estimate the transition between these time regimes, and the fraction of the conductive surface in accordance to the theoretical model (130). In addition to their large collective current, enhanced signal-to-noise ratios, and flow rate independence (in flow detection), composite electrodes hold great promise for incorporating appropriate modifiers within the bulk of the composite matrix.

Closely spaced band electrodes (pairs or triples), with each electrode within the diffusion layer of the other, can be used for studying reactions, in a manner analogous to ring–disk generation–collection and redox recycling experiments (131,132). Unlike with rotating ring–disk electrodes, the product of the reaction at the collector electrode can diffuse back across the narrow gap to the

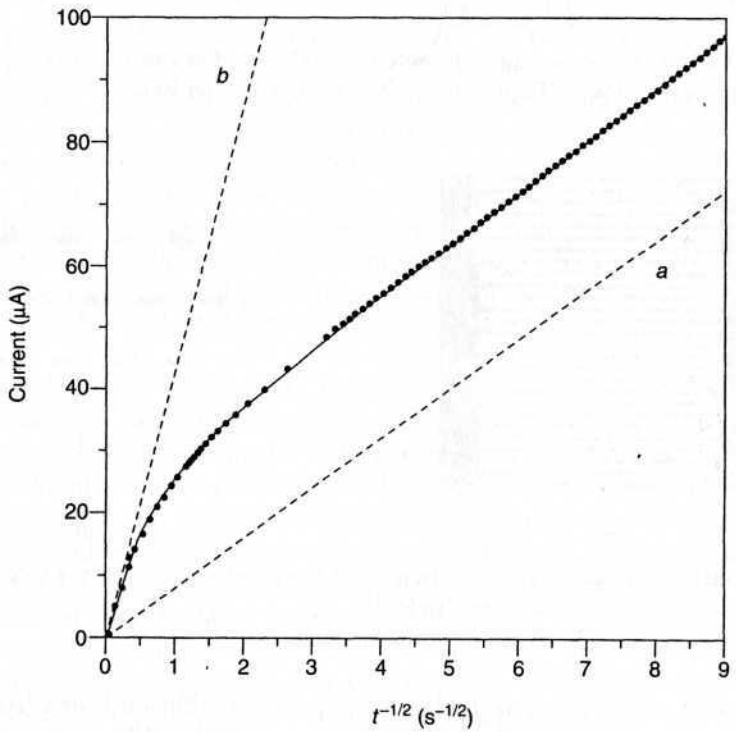

Figure 4.31 Cottrell plot of the chronoamperometric response for 1×10^{-3}M $Ru(NH_3)_6^{3+}$ at a Kel-F/gold composite electrode. Points represent experimental data; the solid line indicates the least-squares fit to theory. Dashed lines indicate theoretical Cottrell plots for a macroelectrode with active area equal to the active area of the composite (*a*) and to the geometric area of the composite (*b*). (Reproduced with permission from Ref. 122.)

generator electrode to give higher collection efficiencies. A typical generation–collection experiment at such an array is illustrated in Figure 4.32. Such electrochemical recycling of a reversible redox couple provides a signal amplification (i.e., higher sensitivity) that cannot be achieved at a single electrode, and indicates great promise for various sensing applications (133,134). The coverage of such closely spaced microelectrodes with conducting polymers can form the basis for novel microelectronic (transistor-like) sensing devices (see Chapter 6). The properties and applications of interdigitated arrays of microband electrodes have been reviewed (133). Ordered arrays, featuring regular disk microelectrode sizes and spacing, have potential applications as sensor arrays or high-density DNA and protein chips (discussed in Chapter 6).

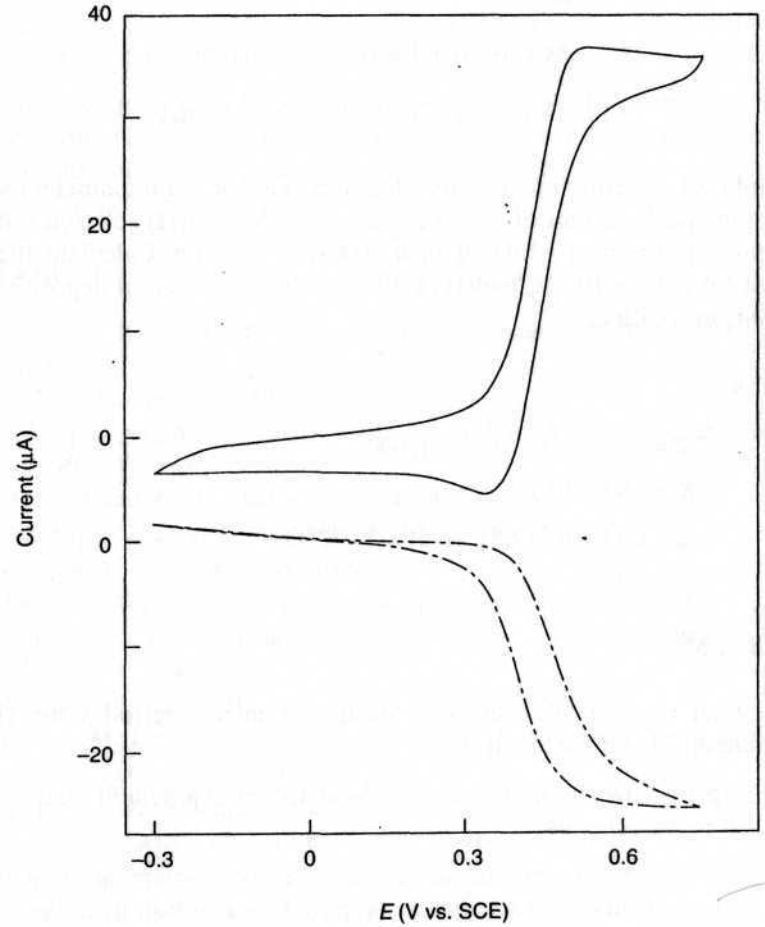

Figure 4.32 Cyclic voltammogram for ferrocene at a 3-μm-wide, 2-μm gap interdigitated microband (solid line). The dotted line represents the current of the collector electrode held at a potential of –0.1 V. (Reproduced with permission from Ref. 132.)

EXAMPLES

Example 4.1 A rotating ring–disk electrode (1600 rpm) yields a disk current of 12.3 μA for the oxidation of a 2×10^{-3} M potassium ferrocyanide solution. Calculate the reduction current observed at the surrounding ring using a 6×10^{-3} M potassium ferrocyanide solution and a rotation speed of 2500 rpm ($N = 0.33$).

Solution From the Levich equation, (4.5), one can calculate first the disk current under the new conditions:

$$i_D/12.3 = K \times (6 \times 10^{-3}) \times (2500)^{1/2} / K \times (2 \times 10^{-3}) \times (1600)^{1/2}$$

$$i_D = 46.125\,\mu A$$

Then, from Eq. (4.8), we can solve for the ring current:

$$i_R = -Ni_D = -0.33 \times 12.125 = -15.221\,\mu A$$

Example 4.2 A rotating mercury film electrode (of 2 mm diameter) yielded a stripping peak current of 2.2 μA for a 1×10^{-8} M lead(II) solution following a 3-min deposition at −1.0 V with a 1600 rpm rotation. Calculate the peak current for a 2.5×10^{-8} M lead(II) solution following a 2-min deposition with a 2500-rpm rotation.

Solution

$$2.2 = K \times (1 \times 10^{-8}) \times 3 \times (1600)^{1/2}$$

$$K = 1.83 \times 10^6$$

$$i_p = 1.83 \times 10^6 (2.5 \times 10^{-8}) \times 2 \times (2500)^{1/2} \qquad i_p = 4.6\,\mu A$$

PROBLEMS

4.1 What are the advantages of using ultramicroelectrodes for electrochemical measurements?

4.2 Explain how chemically modified electrodes can benefit electrochemical measurements.

4.3 Explain why a carbon composite disk electrode offers improved signal-to-background characteristics compared to a carbon disk electrode of the same geometric area.

4.4 Describe why the oxidation of polypyrrole film results in the uptake of an anion from the surrounding solution.

4.5 Derive the Levich equation for the limiting current at the rotating disk electrode [based on combining Eqs. (3.4) and (1.12)].

4.6 How can you use the rotating–ring disk electrode for detecting short-lived intermediate species?

4.7 Explain why an effective compensation of the ohmic drop is essential for diagnostic applications of cyclic voltammetry (e.g., estimating n from ΔE_p).

4.8 Describe the rationale for using electrodes coated with Nafion films for selective detection of the cationic neurotransmitter dopamine in the presence of coexisting interfering anionic ascorbic acid.

4.9 Explain the reason for including the time-consuming oxygen removal step in pulse polarographic measurements of tin ion in juice samples.

4.10 Explain why and how a change in scan rate affects the shape of the cyclic voltammetric response of an ultramicroelectrodes.

4.11 Propose a modified electrode surface suitable for detecting in situ micromolar concentrations of ferric ion in an industrial stream. What are the challenges for such in situ monitoring?

REFERENCES

1. DeAngelis, T. P.; Bond, R. E.; Brooks, E. E.; Heineman, W. R., *Anal. Chem.* **49**, 1792 (1977).
2. Clark, R.; Ewing, A. G., *Anal. Chem.* **70**, 1119 (1998).
3. Mann, C. K., in *Electroanalytical Chemistry*, A. J. Bard, ed., Marcel Dekker, New York, 1969, Vol. 3, p. 57.
4. Silva, S.; Bond, A. M., *Anal. Chim. Acta* **500**, 307 (2003).
5. Wallace, G. G., *Trends Anal. Chem.* **4**, 145 (1985).
6. Newman, A., *Anal. Chem.* **69**, 369A (1997).
7. Matsue, T.; Aoki, A.; Ando, E.; Uchida, I., *Anal. Chem.* **62**, 409 (1990).
8. Bond, A. M., *Modern Polarographic Methods in Analytical Chemistry*, Marcel Dekker, New York, 1980.
9. He, P.; Avery, J.; Faulkner, L. R., *Anal. Chem.* **54**, 1314 (1982).
10. Bond, A. M.; Luscombe, D.; Tan, S. N.; Walter, F. L., *Electroanalysis* **2**, 195 (1990).
11. Wang, J., *Analyst* **119**, 763 (1994).
12. Erickson, K. A.; Wilding, P., *Clin. Chem.* **39**, 283 (1993).
13. Kemula, W.; Kublik, K., *Anal. Chim. Acta* **18**, 104 (1958).
14. Peterson, W., *Am. Lab.* **12**, 69 (1979).
15. Macchi, G., *J. Electroanal. Chem.* **9**, 290 (1965).
16. Kowalski, Z.; Wang, K.; Osteryoung, R.; Osteryoung, J., *Anal. Chem.* **59**, 2216 (1987).
17. Florence, T. M., *J. Electroanal. Chem.* **27**, 273 (1970).

18. Adams, R. N., *Electrochemistry at Solid Electrodes*, Marcel Dekker, New York, 1969.
19. Engstrom, R. C., *Anal. Chem.* **56**, 890 (1984).
20. Albery, W. J.; Hitchman, M., *Ring-Disk Electrodes*, Clarendon Press, Oxford, UK, 1971.
21. McCreery, R. L., "Carbon electrodes: Structural effects on electron transfer kinetics," in A. J. Bard, ed., *Electroanalytical Chemistry*, Marcel Dekker, New York, 1991, Vol. 18.
22. Chen, P.; McCreery, R. L., *Anal. Chem.* **68**, 3958 (1996).
23. Bokros, J. C., *Carbon* **15**, 355 (1977).
24. Fagan, D.; Hu, I.; Kuwana, T., *Anal. Chem.* **57**, 2759 (1985).
25. Van der Linden, W. E.; Dieker, J. W., *Anal. Chim. Acta* **119**, 1 (1980).
26. Wang, J., *Electrochim. Acta* **26**, 1721 (1981).
27. Olson, C.; Adams, R. N., *Anal. Chim. Acta* **22**, 582 (1960).
28. Urbaniczky, C.; Lundstrom, K., *J. Electroanal. Chem.* **176**, 169 (1984).
29. Rice, M.; Galus, Z.; Adams, R. N., *J. Electroanal. Chem.* **143**, 89 (1983).
30. Kalcher, K., *Electroanalysis* **2**, 419 (1990).
31. Csöregi, E.; Gorton, L.; Marko-Varga, G., *Anal. Chim. Acta* **273**, 59 (1993).
32. Feng, J.; Brazell, M.; Renner, K.; Kasser, R.; Adams, R. N., *Anal. Chem.* **59**, 1863 (1987).
33. Edmonds, T., *Anal. Chim. Acta* **175**, 1 (1985).
34. Compton, R. G.; Foord, J. S.; Marken, F., *Electroanalysis* **15**, 1349 (2003).
35. Xu, J.; Granger, M. C.; Chen, Q.; Lister, T. E.; Strojek, J. W.; Swain, G. M., *Anal. Chem.* **69**, 591A (1997).
36. Terashima, C.; Rao, T. N.; Sarada, B. V.; Tryk, D. A.; Fujishima, A., *Anal. Chem.* **74**, 895 (2002).
37. Marken, F.; Paddon, C. A.; Asogan, D., *Electrochem. Commun.* **4**, 62 (2002).
38. Kozlowska, H.; Conway, B.; Sharp, W., *J. Electroanal. Chem.* **43**, 9 (1973).
39. Johnson, D. C.; LaCourse, W., *Anal. Chem.* **62**, 589A (1990).
40. Colon, L.; Dadoo, R.; Zare, R., *Anal. Chem.* **65**, 476 (1993).
41. Cassela, I. G.; Cataldi, T. R.; Salvi, A.; Desimoni, E., *Anal. Chem.* **65**, 3143 (1993).
42. Wang, J.; Lu, J.; Hocevar, S.; Farias, P.; Ogorevc, B., *Anal. Chem.* **72**, 3218 (2000).
43. Wang, J., *Electroanalysis* **17**, 1341 (2005).
44. Wasmus, S.; Kuver, A., *J. Electroanal. Chem.* **461**, 14 (1999).
45. Murray, R. W.; Ewing, A. G.; Durst, R. A., *Anal. Chem.* **59**, 379A (1987).
46. Wang, J., *Electroanalysis* **3**, 255 (1991).
47. Baldwin, R. P.; Thomsen, K. N., *Talanta* **38**, 1 (1991).
48. Zhong, C.; Porter, M. D., *Anal. Chem.* **67**, 709A (1995).
49. Bain, C.; Whitsides, G., *Angew Chem. Int. Ed. Eng.* **28**(4), 506 (1989).
50. Mandler, D.; Turyan, I., *Electroanalysis* **8**, 207 (1996).
51. Piner, R. D.; Zhu, J.; Zu, F.; Hong, S.; Mirkin, C. A., *Science* **283**, 661 (1999).
52. Kumar, A.; Whitesides, G. M., *Appl. Phys. Lett.* **63**, 2002 (1993).
53. Armstrong, F. A.; Wilson, G. S., *Electrochim. Acta* **45**, 2623 (2000).

54. Baughman, R. H.; Zakhidov, A.; de Heer, W. A., *Science* **297**, 787 (2002).
55. Wang, J.; Musameh, M., *Anal. Chem.* **75**, 2075 (2003).
56. Banks, C. E.; Moore, R. R.; Compton, R. G., *Chem. Commun.* **16**, 1804 (2004).
57. Gooding, J. J.; Wibowo, R.; Liu, J. Q.; Yang, W.; Losic, D.; Orbons, S.; Mearns, F. J.; Shapter, J. G.; Hibbert, D. B., *J. Am. Chem. Soc.* ***125***, 9006 (2003).
58. Patolsky, F.; Weizmann, Y.; Willner, I., *Angew Chem. Int. Ed.* **43**, 2113 (2004).
59. Wang, J., *Electroanalysis* **17**, 7 (2005).
60. Lev, O.; Tsionsky, M.; Rabinovich, I.; Glezer, V.; Sampath, S.; Pankratov, I.; Gun, J., *Anal. Chem.* **67**, 22A (1999).
61. Petit-Dominquez, M.; Shen, H.; Heineman, W. R.; Seliskar, C. J., *Anal. Chem.* **69**, 703 (1997).
62. Tsionsky, M.; Gun, G.; Glezer, V.; Lev, O., *Anal. Chem.* **66**, 1747 (1994).
63. Wang, J.; Pamidi, P., *Anal. Chem.* **69**, 4490 (1997).
64. Marx, S.; Zaltsman, A.; Turyan, I.; Mandler, D., *Anal. Chem.* **76**, 120 (2004).
65. Zak, J.; Kuwana, T., *J. Electroanal. Chem.* **150**, 645 (1983).
66. Cox, J.; Jaworski, R.; Kulesza, P., *Electroanalysis* **3**, 869 (1991).
67. Gorton, L., *J. Chem. Soc. Faraday Trans.* **82**, 1245 (1986).
68. Halbert, M.; Baldwin, R., *Anal. Chem.* **57**, 591 (1985).
69. Malinski, T.; Taha, Z., *Nature* **358**, 676 (1992).
70. Wang, J.; Taha, Z., *Anal. Chem.* **62**, 1413 (1990).
71. Karayakin, K., *Electroanalysis* **13**, 813 (2001).
72. Carrette, L.; Friedrich, K. A.; Stimming, U., *Fuel Cells* **1**, 5 (2001).
73. Wang, J., "Voltammetry after nonelectrolytic preconcentration," in A. J. Bard, ed., *Electroanalytical Chemistry*, Marcel Dekker, New York, 1989, Vol. 16, p. 1.
74. Guadalupe, A.; Abruna, H., *Anal. Chem.* **57**, 142 (1985).
75. Arrigan, D. W., *Analyst* **119**, 1953 (1994).
76. Ugo, P.; Moreto, L. M., *Electroanalysis* **7**, 1105 (1995).
77. Prabhu, S.; Baldwin, R.; Kryger, L., *Anal. Chem.* **59**, 1074 (1987).
78. Wang, J.; Martinez, T., *Electroanalysis* **1**, 167 (1989).
79. Oyama, N.; Anson, F. C., *Anal. Chem.* **52**, 1192 (1980).
80. Wang, J.; Lu, Z., *J. Electroanal. Chem.* **266**, 287 (1989).
81. Prabhu, S.; Baldwin, R.; Kryger, L., *Electroanalysis* **1**, 13 (1989).
82. Ugo, P.; Ballarin, B.; Daniele, S.; Mazzocchin, G., *Anal. Chim. Acta* **244**, 29 (1991).
83. Turyan, I.; Mandler, D., *Anal. Chem.* **66**, 58 (1994).
84. Yang, W. R.; Jaramillo, D.; Gooding, J. J.; Hibbert, D. B.; Zhang, R.; Willett, G. D.; Fisher, K., *J. Chem. Commun.* 1982 (2001).
85. Malinski, T.; Ciszewski, A.; Fish, J.; Czuchajowski, L., *Anal. Chem.* **62**, 90 (1990).
86. Sasso, S. V.; Pierce, R.; Walla, R.; Yacynych. A., *Anal. Chem.* **62**, 1111 (1990).
87. Nagy, G.; Gerhardt, G.; Oke, A.; Rice, M.; Adams, R. N., *J. Electroanal. Chem.* **188**, 85 (1985).
88. Wang, J.; Lu, Z., *Anal. Chem.* **62**, 826 (1990).
89. Wang, J.; Wu, H.; Angnes, S., *Anal. Chem.* **65**, 1893 (1993).
90. Wang, J.; Tuzhi, P., *Anal. Chem.* **58**, 3257 (1986).

91. Sittampalam, G.; Wilson, G., *Anal. Chem.* **55**, 1608 (1983).
92. Ohsaka, T.; Hirokawa, T.; Miyamoto, H.; Oyama, N., *Anal. Chem.* **59**, 1758 (1987).
93. Wang, J.; Golden, T., *Anal. Chem.* **61**, 1397 (1989).
94. Cheng, Q.; Brajter-Toth, A., *Anal. Chem.* **64**, 1998 (1992).
95. Bidan, G., *Sensors and Actuators B* **6**, 45 (1992).
96. Kanatzidis, M., *Chem. Eng. News* 36 (Dec. 3, 1990).
97. Ikariyama, T.; Heineman, W. R., *Anal. Chem.* **58**, 1803 (1986).
98. Ivaska, A., *Electroanalysis* **3**, 247 (1991).
99. Teasdale, P.; Wallace, G., *Analyst* **118**, 329 (1993).
100. Liu, H.; Kameoka, J.; Caplewski, D. A.; Craighead, H. G., *Nano. Lett.* **4**, 671 (2004).
101. Martin, C. R., *Science* **266**, 1961 (1994).
102. Ramanathan, K.; Bangar, M. A.; Yun, M.; Chen, W.; Mulchandani, A.; Myang, N. V. *Nano. Lett.* **4**, 1237 (2004).
103. Piletsky, S. A.; Turner, A. P., *Electroanalysis* **14**, 317 (2002).
104. Malitesta, C.; Losito, I.; Zambonin, P. G., *Anal. Chem.* **71**, 1366 (1999).
105. Wightman, R. M., *Science* **240**, 415 (1988).
106. Wightman, R. M., *Anal. Chem.* **53**, 1125A (1981).
107. Bond, A. M., *Analyst* **119**, R1 (1994).
108. Zoski, C. G., *Electroanalysis* **14**, 1041 (2002).
109. Kennedy, R.; Huang, L.; Atkinson, M.; Dush, P., *Anal. Chem.* **65**, 1882 (1993).
110. Cahill, P. S.; Walker, Q. D.; Finnegan, J. M.; Mickelson, G. E.; Travis, E. R.; Wightman, R. M., *Anal. Chem.* **68**, 3180 (1996).
111. Bedioui, F.; Villeneuve, N., *Electroanalysis* **15**, 5 (2003).
112. Fan, F.; Kwak, J.; Bard, A. J., *J. Am. Chem. Soc.* **118**, 9669 (1996).
113. Anderson, B. B.; Ewing, A. G., *J. Pharm. Biomed. Anal.* **19**, 15 (1999).
114. Andrieux, C. P.; Hapiot, P.; Saveant, J. M., *Electroanalysis* **2**, 183 (1990).
115. White, R. J.; White, H. S., *Anal. Chem.* **77**, 215A (2005).
116. Heinze, J., *Angew. Chem. (Engl. Ed.)* **32**, 1268 (1993).
117. Penner, R.; Lewis, N., *Chem. Ind.* 788 (Nov. 4, 1991).
118. Watkins, J.; Chen, J.; White, H.; Abruna, H.; Maisonhaute, E.; Amatore, C., *Anal. Chem.* **75**, 3962 (2003).
119. Watkins, J. J.; Zhang, B.; White, H. S., *J. Chem. Educ.* **82**, 712 (2005).
120. Arrigan, D. W. M., *Analyst* **129**, 1157 (2004).
121. Shao, Y.; Mirkin, M. V.; Fish, G.; Kokotov, S.; Palankar, D.; Lewis, A., *Anal. Chem.* **69**, 1627 (1997).
122. Tallman, D. E.; Petersen, S. L., *Electroanalysis* **2**, 499 (1990).
123. Thormann, W.; van den Bosch, P.; Bond, A. M., *Anal. Chem.* **57**, 2764 (1985).
124. Feeny, R.; Kounaves, S. P., *Electroanalysis* **12**, 677 (2000).
125. Weisshaar, D. E.; Tallman, D. E., *Anal. Chem.* **55**, 1146 (1983).
126. Wang, J.; Brennsteiner, A.; Sylwester, A. P., *Anal. Chem.* **62**, 1102 (1990).
127. Deutscher, R.; Fletcher, S., *J. Electroanal. Chem.* **239**, 17 (1988).
128. Penner, R. M.; Martin, C. R., *Anal. Chem.* **59**, 2625 (1987).

129. Hulteen, J. C.; Martin, C. R., *J. Mater. Chem.* **7**, 1075 (1997).
130. Gueshi, T.; Tokuda, K.; Matsuda, H., *J. Electroanal. Chem.* **89**, 247 (1978).
131. Bard, A. J.; Crayton, J.; Kittlesen, G.; Shea, T.; Wrighton, M. S., *Anal. Chem.* **58**, 2321 (1986).
132. Niwa, O.; Morita, M.; Tabei, H., *Anal. Chem.* **62**, 447 (1990).
133. Niwa, O., *Electroanalysis* **7**, 606 (1995).
134. Thomas, J.; Kim, S.; Hesketh, P.; Halsall, H. B.; Heineman, W. R., *Anal. Chem.* **76**, 2700 (2004).